

Advanced Photoresponsive Materials Using the Metal–Organic Framework Approach

Ritesh Haldar, Lars Heinke,* and Christof Wöll*

When fabricating macroscopic devices exploiting the properties of organic chromophores, the corresponding molecules need to be condensed into a solid material. Since optical absorption properties are often strongly affected by interchromophore interactions, solids with a well-defined structure carry substantial advantages over amorphous materials. Here, the metal–organic framework (MOF)-based approach is presented. By appropriate functionalization, most organic chromophores can be converted to function as linkers, which can coordinate to metal or metal-oxo centers so as to yield stable, crystalline frameworks. Photoexcitations in such chromophore-based MOFs are surveyed, with a special emphasis on light-switchable MOFs from photochromic molecules. The conventional powder form of MOFs obtained using solvothermal approaches carries certain disadvantages for optical applications, such as limited efficiency resulting from absorption and light scattering caused by the (micrometer-sized) powder particles. How these problems can be avoided by using MOF thin films is demonstrated.

In recent years, a particularly attractive and novel strategy has become available for the fabrication of photoresponsive, porous, and crystalline molecular solids from appropriately functionalized chromophoric linkers. The crystallinity of these materials allows a rather straightforward description and analysis using theoretical methods, thus tremendously accelerating the design of novel materials. This new class of crystalline molecular solids is referred to as metal–organic frameworks, MOFs (or porous coordination polymers, PCPs).^[1] MOFs are constructed from metal-/metal-oxo nodes and organic linkers (Figure 1). The incorporation of photoactive species into MOFs may be realized by using them as linkers (method L) or attaching them to a linker (method A), as shown in Figure 1a. In addition, the porosity of MOFs allows the loading of

chromophoric compounds as guests (method G) into the pores of this interesting framework material.

In this review article, we mainly focus on organic photoactive species, which are either simply loaded as guests into porous MOFs or used after appropriate functionalization as building blocks for the construction of the framework (methods L, A, and G).^[2] It is important to note that in the context of photoresponsive behavior, MOFs carry a potential which by far exceeds that of nonporous coordination polymers. This is because simple loading of guest/solvent molecules of different size/polarity/functionality in the MOF pores can impart a large optical response, which is useful, e.g., for sensing applications.^[3] As an example, the solvent-dependent optical response or solvatochromism^[4] is illustrated in Figure 1b. Such effects cannot be realized for nonporous coordination polymers.


The different types of photoresponsive molecules addressed in this review can be grouped into two classes. The first contains molecules where the structure remains essentially unchanged upon light-induced electronic excitation, and the second contains molecular species that change their structure or conformation upon absorption of photons (molecular switches).

Light with a wavelength in the range 200–800 nm (6.2–1.5 eV) can excite a molecule to a transient excited electronic state. The transient state then decays to a low-energy state, either the parent ground state or another longer-lived excited state. Decay time scales are in the range 10^{-12} – 10^1 s, and the released energy can be radiative or nonradiative in nature. For many applications, nonradiative energy loss is unwanted,

1. Introduction

Photoactive organic molecules display a huge variety of interesting properties, including luminescence, energy harvesting, photon up- or downconversion, nonlinear optical properties, and photoinduced switching of conformations. In addition to their use in fundamental studies on light–matter interaction, such chromophores can be employed to fabricate materials with exciting properties and to realize applications in a variety of different fields. Obtaining photoactive materials from organic chromophores can be achieved via different methods, starting from condensation to yield molecular solids or using appropriate liquid or solid solutions. Materials that are more robust can be obtained by adding appropriate side groups and then coupling those using suitable chemistries, thus yielding polymers.

Dr. R. Haldar, Dr. L. Heinke, Prof. C. Wöll
Karlsruher Institut für Technologie (KIT)
Institut für Funktionelle Grenzflächen (IFG)
Hermann-von-Helmholtz-Platz 1, 76344 Eggenstein-Leopoldshafen,
Germany
E-mail: Lars.Heinke@KIT.edu; Christof.Woell@KIT.edu

 The ORCID identification number(s) for the author(s) of this article can be found under <https://doi.org/10.1002/adma.201905227>.

© 2019 The Authors. Published by WILEY-VCH Verlag GmbH & Co. KGaA, Weinheim. This is an open access article under the terms of the Creative Commons Attribution License, which permits use, distribution and reproduction in any medium, provided the original work is properly cited.

DOI: 10.1002/adma.201905227

but it can occur through quenching of the primary excitation at structural defects and excitations of lattice vibrations.

Typical applications of chromophoric materials are based on fluorescence, phosphorescence, or charge separation. Chromophores with extended conjugated π -systems, such as the ones shown in **Figure 2a**, are well suited for such purposes. The photophysical properties of photoactive molecules may be strongly affected when they are assembled into a material. Such intermolecular effects already play a role for solvated individual species (solvatochromism),^[7,8] but they can strengthen in the case of molecular solids. We point out in this review that the different architectures available with the MOF-based approach allow precise control over these intermolecular couplings between adjacent chromophores.

We will use the term photoswitching for molecular species with two or more stable or metastable molecular states, between which transitions can be induced by photon absorption (**Figure 2b**). Often, there is one thermodynamically stable isomer, the ground state, and an excited state that thermally isomerizes back to the ground state. We will only consider cases where the time constants for the backswitching is at least several seconds or minutes, thus allowing for a more detailed investigation of the state and the ability to render functionality to the corresponding material. Such MOF switchable materials are reviewed in Section 4. Note, however, that a clear discrimination between the two cases is not always possible. As an example, spiropyran undergoes photoisomerization to merocyanine (MC), which is fluorescent.^[9]

2. MOFs, MOF Thin Films, and Surface-Anchored MOFs (SURMOFs)

MOFs are presently a topic of intense research. With more than 100 000 compounds already described in the literature, this class of materials is too rich in number and too diverse in nature to include all the details in the context of this review. Readers are referred to recent overview articles describing the state of the art in this field.^[10] For conventional MOF applications like gas storage,^[11] pressure-swing adsorption separation,^[12] or catalytic conversion,^[13] the powder form of these porous materials obtained from the typical solvothermal synthesis of these compounds is very efficient. However, powders or pellets made from porous materials are not well suited for optical applications, since scattering effects may severely hamper their photophysical characterization.

For these purposes, MOF thin films or SURMOFs^[14] are much better suited, as illustrated in **Figure 3**. SURMOFs are also well suited as model systems for more conventional applications, e.g., for uptake and diffusion studies.^[15] Thin MOF films can be prepared using various methods, such as vapor-assisted growth^[16] and chemical vapor deposition^[17] (**Figure 3a,b**). The huge interest in MOF thin films has resulted in the development of a variety of additional coating schemes, including various one-pot synthesis and sol-gel methods,^[18] as well as inkjet printing,^[19] employing polymer composites^[20] and spin-coating of MOF nanoparticles. A very controlled MOF thin film synthesis can be achieved by using a layer-by-layer (lbl) assembly, resulting in SURMOFs (**Figure 3c**).^[14b] SURMOFs have many



Ritesh Haldar received his master's degree in inorganic chemistry at the University of Pune, India and did his Ph.D. in 2015 under the supervision of Prof. Tapas Kumar Maji at Jawaharlal Nehru Centre for Advanced Scientific Research (JNCASR), Bangalore, India. He joined the Karlsruhe Institute of Technology (KIT) as an Alexander von Humboldt (AvH) postdoctoral fellow mentored by Prof. Christof Wöll. His current research area is metal-organic thin films and their applications in optoelectronics.



Lars Heinke studied physics in Greifswald and Leipzig and obtained his Ph.D. in the group of Jörg Kärger in 2009. After postdoctoral stays at the Fritz-Haber Institute, Berlin, and at the Lawrence Berkeley National Laboratory, California, he joined the Institute of Functional Interfaces at the KIT as group leader. In 2015, he finished his habilitation mentored by Christof Wöll. His research foci comprise functional nanoporous films and their physical properties; especially, conduction and diffusion as well as photoresponsive, smart coatings.



Christof Wöll studied physics at the University of Göttingen and received his Ph.D. (physics) from Göttingen University in 1987. After a postdoctoral stay at IBM Research Laboratory, San Jose, CA, he joined Heidelberg University in 1989. After his Habilitation (1992) he was a Heisenberg Fellow of the Deutsche Forschungsgemeinschaft (DFG). In 1997, he was appointed full professor (physical chemistry) at Bochum University. In 2000, he founded the collaborative research center SFB588 "Metal-Substrate Interactions in Heterogeneous Catalysis." In 2009, he became director of the Institute of Functional Interfaces at Karlsruhe Institute of Technology (KIT). His research focuses on fundamental processes in surface physics and surface chemistry, including surface-supported metal-organic framework thin films (SURMOFs).

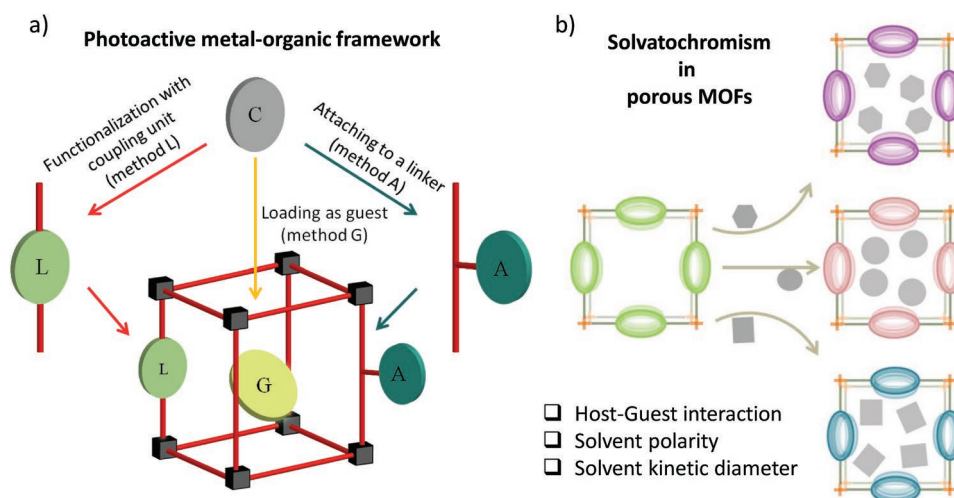


Figure 1. a) A schematic representation of different ways to integrate photoactive components in a metal–organic framework (MOF); b) schematic of a guest (solvent) mediated optical changes in porous MOFs, described as solvatochromism.

unique features, such as a very small surface roughness^[21] and small defect densities.^[22] They are monolithic and have a well-defined, controllable thickness, which can be adjusted to the targeted application and exhibit high optical transparency.^[23]

The advantage of thin films/SURMOFs becomes clear when considering that the extent of the response of a photoactive material to illumination is proportional to the light absorption efficiency. However, in bulk MOF materials consisting of particles with sizes typically in the range from 100 nm to a few micrometers, the light penetration depth depends on the absorption cross section, which for efficient absorbers may fall in the regime of the MOF particle sizes. Absorption is then

often confined to the outer surface of the MOF material, and a reliable photophysical characterization of powder MOF materials will become very challenging or even impossible.

The impact of the material morphology on the recorded absorption spectrum is illustrated in **Figure 4a**, where we compare the data recorded for a homogenous film to that of the corresponding powder material. Although having identical intrinsic material properties, the substantial inhomogeneity of the powder affects the absorption spectrum, reduces the obtained absorbance intensity, and broadens the absorption peaks. **Figure 4b** shows examples of absorption spectra recorded in transmission mode for two types of MOF

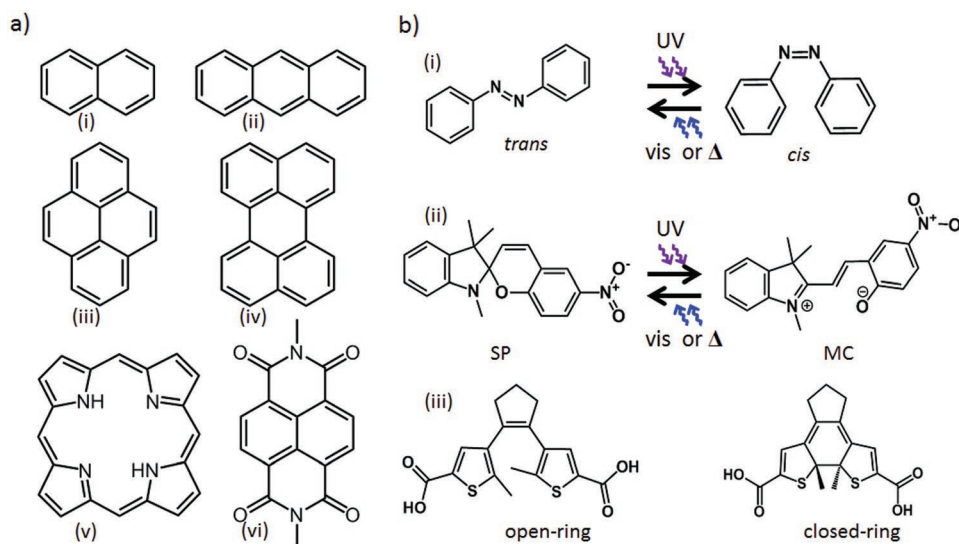


Figure 2. Photoresponsive molecules. a) Photoexcitable chromophores used as MOF linkers to study photoexcited state: (i) naphthalene, (ii) anthracene, (iii) pyrene, (iv) perylene, (v) porphyrin, and (vi) naphthalenediimide. b) Photoswitchable molecules such as azobenzene, spiropyran, or diarylethene can be switched between two stable states. Azobenzene (i, AB) undergoes light-induced *trans*–*cis* isomerization; Spiropyran (ii, SP) isomerizes to merocyanine (MC), and diarylethene (iii, DAE) undergoes light-induced ring-opening and ring-closing isomerizations. Along with the structural changes, the electronic structure and dipole moments change, which are 0 D for *trans* and 3 D for *cis* (plain) AB as well as 4–6 D for SP and 14–18 D for MC.^[5] DAE may also change its dipole moment.^[6]

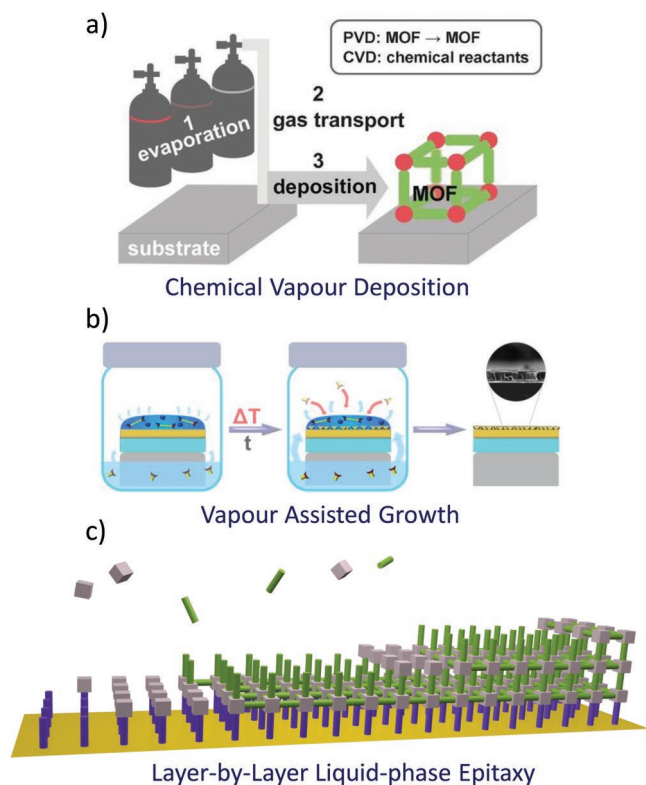


Figure 3. Methods of MOF film growth. a) Chemical vapor deposition of MOF. Reproduced with permission.^[17b] Copyright 2016, Wiley-VCH. b) Vapor-assisted growth. Reproduced with permission.^[16] Copyright 2018, American Chemical Society. c) Layer-by-layer film growth by liquid-phase epitaxy.

films deposited on quartz substrates: a drop-cast film of a MOF powder (blue) and a corresponding SURMOF (wine). For this illustration, we use a $\text{Zn}_2(\text{adc})_2(\text{dabco})$ MOF (adc = 9,10-anthracenedicarboxylate; dabco = 1,4-diazabicyclo[2.2.2]octane).^[24] For the SURMOF thin-film spectrum, all peaks are as sharp as in the corresponding adc linker solution (gray), and the vibronic pattern is well resolved. For the powder MOF drop cast, on the other hand, the peak profiles are broadened due to scattering effects, the relative intensities of the peaks are changed, and the overall signal-to-noise ratio is substantially reduced. For optical applications of MOFs, therefore, thin films and SURMOFs are highly beneficial, in particular in the context of more advanced applications, like transient optical absorption spectroscopy.^[25]

3. Short-Lived Photoexcited State of Chromophores

The photoexcited states of MOF linkers/guests can have different relaxation paths, which can lead to (A) fluorescence, (B) phosphorescence, or (C) charge separation. The time scale and quantum yield (QY) of the A and B processes are different, the complexity of the excited-state relaxations is huge, and there is a substantial influence of the chemical environment. Particularly, intermolecular interactions can play a significant role. For

example, the energy stored in the molecule after absorption and initial vibronic relaxation can be transferred to neighboring chromophores with suitable energy states by energy transfer mechanisms, such as Förster or Dexter resonance energy transfer. In addition, the excited state can electronically couple with the neighboring chromophore to result in a new excited state (excimer/excplex) that is delocalized over more than one molecule.^[26]

Studies on such photoexcitation decay processes are of substantial importance for understanding fundamental principles and for realizing applications, and the amount of available literature is fairly large. Organic polymers,^[27] covalent organic frameworks (COFs),^[28] dendrimers,^[29] and molecular state studies^[30] often appear in the literature. The primary motivation for such photophysical studies is to build artificial photosynthetic materials, solid-state lighting for displays, and optical sensors. In this context, the photoexcited state of the chromophoric linker in MOF is special for the following three reasons: (i) The chromophore spatial disposition is fixed and direct information on the geometry is available, which allows us to understand the chemical and physical environment of the ground and excited state of the chromophore; (ii) the exact distance of the neighboring chromophores is available, and hence excited/ground-state electronic coupling and energy transport rate calculations are possible; and (iii) isorecticular chemistry of MOF helps create similar assemblies for different chromophores, e.g., the control of chromophore–chromophore distances is allowed, which is nearly impossible in self-assembled organic structures. These three situations are illustrated in **Figure 5**, where energy donor–acceptor chromophoric linkers are positioned at a fixed distance from the substrate by employing the SURMOF approach. Considering these points, MOFs can be regarded as an excellent platform to realize model systems for photophysical and photochemical processes, as well as for photosynthesis. An insightful review by So et al.^[32] and a concept article by Williams et al.^[33] described the importance of MOFs in this regard.

In the literature, the beneficial properties of chromophoric MOFs for diverse applications within the context of “luminescent,” “light harvesting,” “tunable emission,” “sensing,” “recognition,” “highly emissive,” “explosive detection,” “lasing,” and “light emitting” have been described in a rather large set of works, as can be seen from the bar diagram shown in **Figure 6**. There, we have plotted the number of papers containing the keywords “luminescence,” “sensing,” “exciton,” and “energy transfer” in connection with “metal–organic frameworks.” The increasing numbers for the term “sensing” clearly demonstrate potential real-time applications based on MOFs (“sensing” is broadly used in this search, as it can also include other physical or chemical properties of MOFs). The excellent reviews by Kreno et al.^[34] and more recently by Lustig et al.^[35] elaborately explained the strategies undertaken for MOF-based sensing material fabrication and the state-of-the-art research in this direction.

It is interesting to note that the number of publications highlighting “energy transfer” or “exciton” in the title is rising substantially slower than those using terms more related to applications: “luminescence” and “sensing” (**Figure 6**). This observation indicates that research on MOF’s basic photophysical properties is

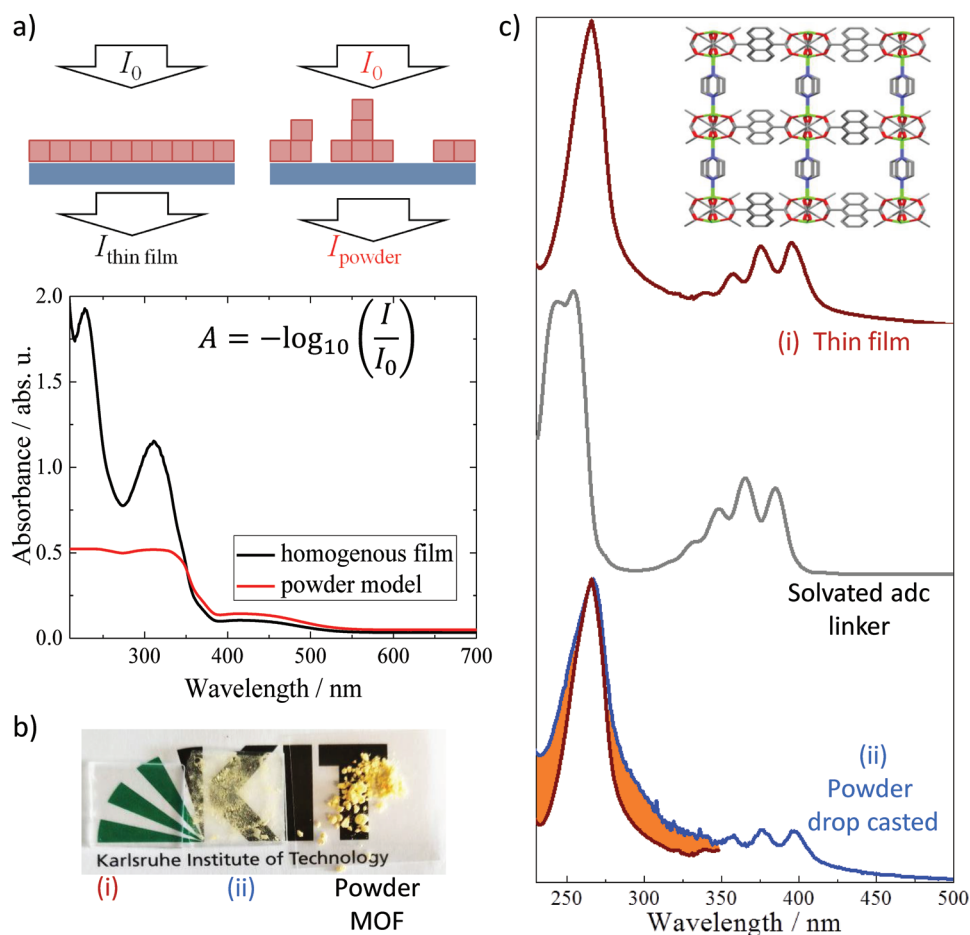


Figure 4. a) Simplified scheme of the structure within a homogeneous MOF thin film, compared to that of multilayer of powder particles of the identical material. Simulations of the corresponding optical absorption spectra are shown below. Due to the nonhomogeneous thickness, drastic changes of the overall absorbance are obtained. b) Photographs of a layer-by-layer grown thin film (i), drop-cast MOF powder (ii), and MOF powder. c) Normalized absorption spectra of solvated adc linker (20×10^{-6} m in ethanol, gray), drop-cast $\text{Zn}_2(\text{adc})_2(\text{dabco})$ MOF powder (blue), and thin film (wine) recorded in transmission mode. The orange marked area shows the unwanted broadening in the drop-cast powder sample compared to the transparent thin film. Inset: 3D structure of $\text{Zn}_2(\text{adc})_2(\text{dabco})$ MOF, the thin film was grown by a layer-by-layer approach using a pump method at 60°C and has a thickness of ≈ 200 nm. Powder with an average particle size of 1–10 μm was drop-cast on quartz glass.

still in an early state, whereas application-based research is proceeding at a substantial pace.

Some of the previous work related to chromophoric MOFs have been reviewed previously, including a road map toward real-time applications, e.g., see the paper by Ameloot and co-workers on luminescent MOFs^[36] and on optoelectronic applications.^[37] Also, luminescent MOF-based sensors,^[34,35,38] luminescence of MOFs, energy transfer and light harvesting,^[31] and the lasing properties^[39] of chromophoric MOFs have been reviewed. Detailed reviews by Chen,^[40] Allendorf,^[41] and Li and co-workers^[42] on luminescent MOFs provide an illustrative account of the research progress in these directions.

In the present overview, we will focus on more fundamental properties applied to the goal of tuning the photoexcitation process and describing the exciton dynamics. We selected some of the most instructive examples for developing important concepts toward enhancement and tuning of photoluminescence properties.

3.1. Photoexcitation of Chromophoric MOFs: Linker-Based Emission

Metal-coordination-induced rigidity in the chromophoric linker (method-L) can have a large impact on the optical properties. This is because the lattice vibration/stretching modes which can affect light absorption/emission efficacy are substantially reduced in the solid, coordinated state compared to the molecular (solvated) state. In 2007, Allendorf and co-workers first described a case in which fluorescence efficiency of the linker (stilbene) was enhanced in MOF, compared to its solvated state.^[43] The fluorescence spectra of the two MOF structures, constructed by linking trans-4,4'-stilbene dicarboxylic acid with Zn(II), were studied in single crystal state and compared with non-coordinated state of the linker. In the later years, this concept of rigidifying chromophore configuration to achieve improved luminescence properties has been studied in great detail and some of the key findings are described in the following discussion.

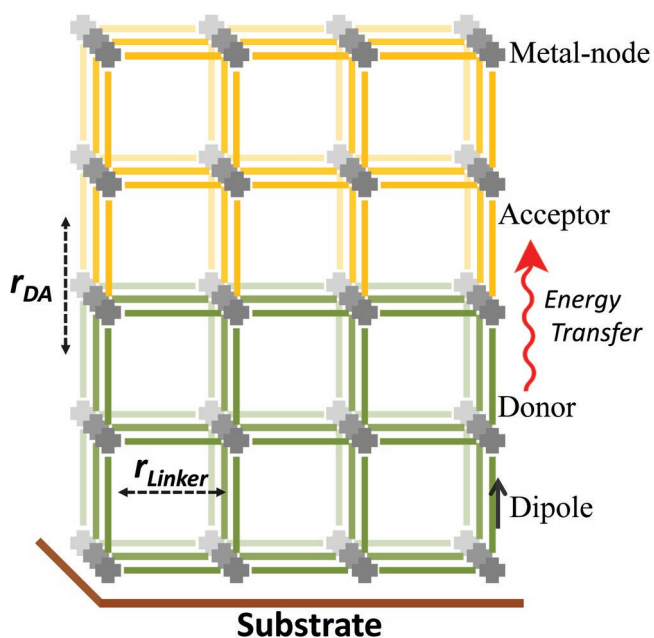


Figure 5. A schematic of layer-by-layer grown hetero-multilayer^[31] SURMOF having energy donor and acceptor chromophoric linkers (solid bars) positioned at fixed distances (r_{DA}) in a crystalline lattice. The strict periodic arrangement also fixes interlinker distance (r_{linker}) and transition dipole orientations.

In 2010, Rosseinsky and co-workers^[44] reported a pyrene-linker-based indium (In)-MOF with a fluorescence quantum yield of 6.7% and a lifetime in the range of milliseconds. In this MOF structure, the pyrene linkers are spatially well separated, and the observed blue fluorescence was ascribed to a ligand-centered singlet-state emission. Interestingly, the fluorescence lifetime of the free linker in the solid state was lower

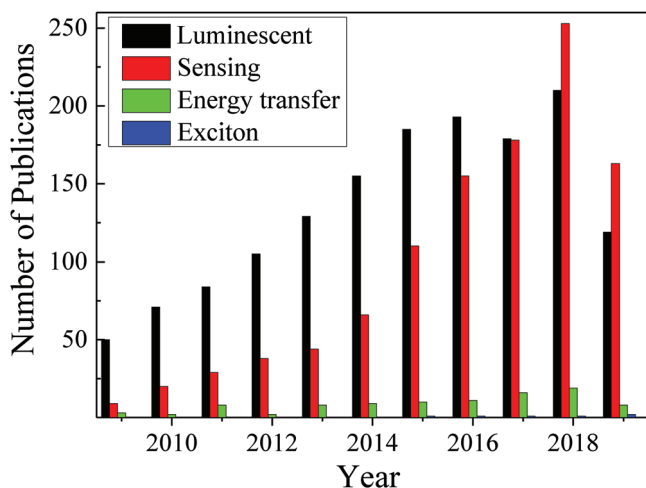


Figure 6. Number of publications with titles having the keywords “luminescent,” “sensing,” “exciton,” and “energy transfer” in connection with “metal–organic frameworks,” “MOF,” or “coordination polymer” published during the past ten years (until August, 2019), according to “Web of Science.” Search details: Luminescent = luminescent, tunable emission, highly emissive, lasing, light emitting; Sensing = sensing, recognition, explosive detection; Energy transfer = energy transfer, light harvesting; Exciton = exciton diffusion, excited-state dynamics.

than in the MOF, indicating reduced nonradiative relaxation paths in the latter case, thus advocating the advantages of a MOF structure in the assembly of luminescent molecules. A few years later, Dincă and co-workers demonstrated a coordination-induced aggregation phenomenon to enhance the photoluminescence quantum yield and lifetime of MOF-based materials.^[45] A chromophore tetraphenylethylene (TPE), well known for its beneficial aggregation-induced emission (AIE) property, was introduced as a MOF linker. The four phenyl rings of TPE lose the π -conjugation in the isolated state due to the free rotation around the C–C bond, as shown in Figure 7a. Close contact upon aggregation freezes this rotation and thus brings back the conjugated structure, which is highly emissive. In this work, high-intensity and long-lived luminescence was obtained by tethering the TPE linker by coordination bonds, thus restricting the phenyl group rotation. A detailed theoretical study revealed a high-energy barrier for phenyl-rotation, which resulted in bright luminescence.^[46,47] Further improvement was reported in a later investigation by Zhou and co-workers for a zirconium (Zr) MOF using a modified linker based on an identical TPE core. They achieved a fluorescence quantum yield of $\approx 100\%$ under inert conditions (Figure 7b,c).^[48] These intriguing results demonstrate the huge potential of coordination-induced emission in the field of display technology (solid-state lighting technology, see also ref. [42]). However, it is worth mentioning that high quantum yield is not the only necessary criterion for solid-state lighting technology. For example in the context of electroluminescent materials,^[49] electron–hole mobility is another key factor and in the context of organic light-emitting diodes (OLEDs) more sophisticated chromophores exhibiting thermally activated delayed fluorescence (TADF)^[50] are of pronounced interest. Such examples realized by chromophoric MOFs will be discussed in a later section of this review.

In the context of TPE-based luminescence, Li and co-workers showed that enhanced conjugation in the TPE core can be used to reduce the highest occupied molecular orbital–lowest unoccupied molecular orbital (HOMO–LUMO) energy gap, and thus the luminescent color, while maintaining high fluorescence quantum yields of $\approx 95\%$.^[51] Note, however, that all the examples discussed above (except ref. [43]) have been obtained for MOF powders, which lack the processibility required for device fabrication.

In this context, a recent report on SURMOF, with MOF thin layers based on a TPE-dicarboxylate linker grown on transparent substrates, represents a substantial step forward.^[52] Due to the close packing of the linkers in the MOF, the phenyl group rotation was strongly reduced, and the Zn-TPE MOF thin film showed bright green emission with a fluorescence lifetime of ≈ 3.8 ns and a fluorescence quantum yield of $\approx 34\%$. Such a bright emissive MOF coating with controllable film thickness is an important advancement toward solid-state display technologies.

Another very interesting class of highly fluorescent chromophores, core-substituted naphthalenediimide (cNDI), can also be deposited as MOF thin films.^[53] This was the first case where crystal structure prediction (CSP) was employed to tune the photophysical properties of a chromophoric MOF material. When the first cNDI linker was assembled to yield the corresponding SURMOF, the resulting chromophoric assembly was dark, that is, a so-called H-aggregate was realized.^[53a] A

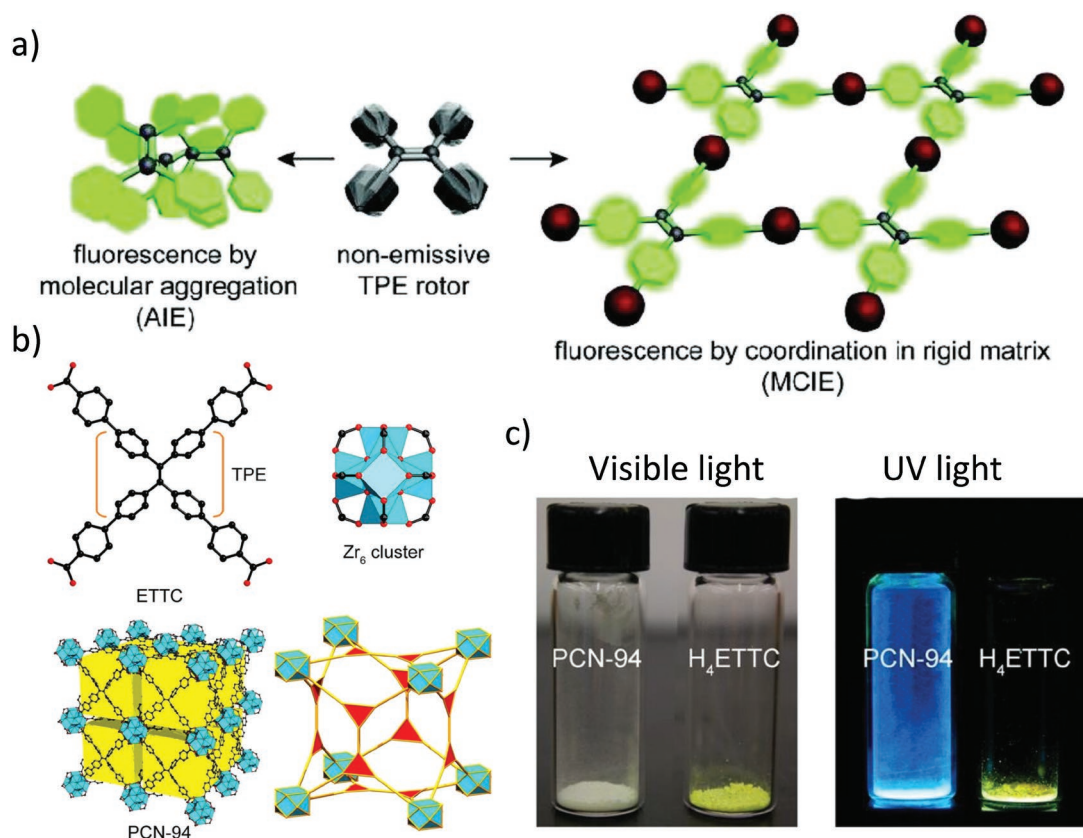


Figure 7. a) Turn-on fluorescence in tetraphenylethylene induced by aggregation and coordination (in MOF). Reproduced with permission.^[45] Copyright 2011, American Chemical Society. b) Structure of the linker ETTC, Zr₆ cluster, and topology of the MOF PCN-94. c) Photographs of H₄ETTC linker and PCN-94 under visible and UV-light. b,c) Reproduced with permission.^[48] Copyright 2014, American Chemical Society.

computational analysis confirmed the existence of a parallel arrangement of the corresponding transition dipole moments, where the photoexcitation energy decays nonradiatively due to forbidden electronic transition.^[53b] Since the goal was to realize a J-aggregate with bright, long-lived fluorescence having large delocalization of excitation energy, the chemical structure of the cNDI linker was slightly modified by attaching a so-called steric control unit (SCU). Although this change did not affect the overall structure (topology and lattice constant) for the corresponding MOF, the relative angle of the transition dipoles was different for different SCUs. After developing a straightforward computational method, it was possible to determine a suitable SCU, out of a library of 20 possible species, for which J-aggregate formation was predicted. This crystal structure prediction strategy of the photoexcited state is of substantial interest concerning the tuning of bandgaps and other photophysical properties. This approach is only possible when using the MOF strategy for assembling the chromophores. We expect that similar concepts will allow for the realization of SURMOFs that are also suitable for the development of solid-state organic light-emitting materials.

There are numerous other reports on luminescent MOFs assembled from chromophoric linkers based on, for example, biphenyl, naphthalene, anthracene, perylene, etc. (see review).^[41,54,55]

On many occasions, the fluorescence observed in MOFs was described as linker based or ligand-to-metal or metal-to-ligand CT based (see later Section 3.3.1), and complete

photophysical characterization was not performed.^[56,57] It is often the case that the MOF emission/absorption spectra were compared to the solid-state free-linker spectra,^[56,58] and straightforward conclusions were drawn without considering the aggregated state of the free linker in the solid state. Nevertheless, it is important to consider the solution-state free-linker spectra/photophysics to rationally describe the effect of MOF structure on the chromophore photophysics. Furthermore, in terms of lifetime and quantum yield, the examples of pyrene and TPE-based MOFs discussed before have remained unmatched so far.

In addition to the short-lived (pico-nanosecond) photoexcited singlet state, long-lived or phosphorescence from the triplet excited state is an exciting aspect, which carries a huge potential for applications in organic light-emitting diodes.^[59] It is worth noting that rare-earth metal-based MOFs do show long-lived, high quantum yield fluorescence, but those are excluded from the present discussion.^[60] Regarding linker-based long-lived phosphorescence in MOFs, only a few cases have been published. In 2014, Sun and co-workers reported a second-timescale emission lifetime in a tri(4-imidazolylphenyl) amine (tipa) linker-based Zn(II) and Cd(II) MOF.^[61] They observed that, upon excitation by 365 nm light at 77 K, both MOFs exhibited delayed fluorescence attributed to triplet-state emission from the tipa linker. Later, for a MOF-5-based structure (Zn-terephthalate), Yan and co-workers^[62] observed

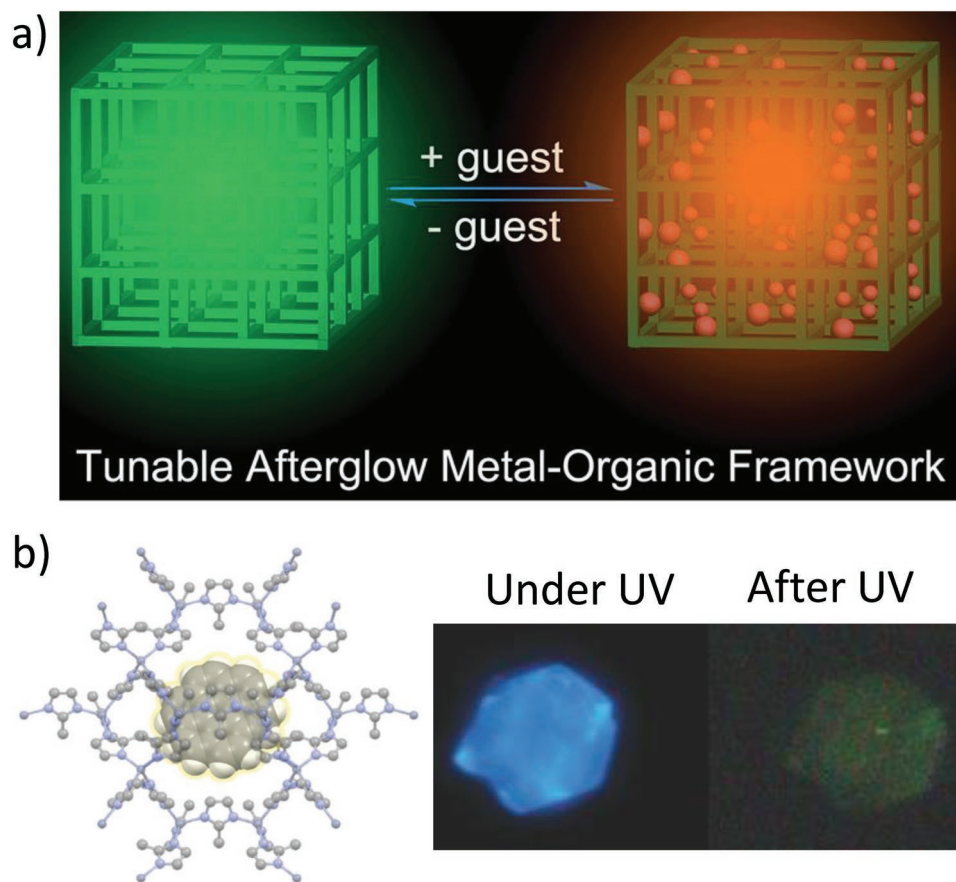


Figure 8. a) A schematic of MOF-5 (Zn-terephthalate) showing tunable afterglow depending on the accommodation of a guest. Reproduced under the terms of the Creative Commons Attribution 3.0 Unported Licence (<https://creativecommons.org/licenses/by/3.0/>).^[62] Copyright 2016, The Royal Society of Chemistry. b) (Left) Structure of a coronene-encapsulated ZIF-8 pore^[63] and (right) photographs of coronene@ZIF-8 under UV illumination and immediately after switching the UV light off. Reproduced with permission.^[63] Copyright 2016, Wiley-VCH.

a lifetime of 0.47 s for phosphorescence at room temperature. Most remarkably, the phosphorescence color was found to be tunable by different guest solvents, as the host–guest structural dynamics played a crucial role in the stabilization of the triplet excited state of the terephthalate linker (**Figure 8a**).

3.2. Photoexcitation of Chromophoric MOFs: Guest-Based Emission

Not only the MOF linkers but also the encapsulated guest can be highly emissive with phosphorescence. An interesting case is presented by Adachi and co-workers, in which a coronene molecule was encapsulated in the pores of a ZIF-8 pore. For this host–guest system at room temperature, phosphorescence with a lifetime of 22 s was observed (**Figure 8b**).^[63] In this case, the encapsulated coronenes in ZIF-8 pores are isolated, and the absence of direct coronene–coronene interactions strongly reduced quenching effects. In a related approach, a Zr-based UiO-68 MOF based on a triphenyldicarboxylate-diphenylamine (tpdc-dpa) linker was reported to exhibit TADF.^[64] For the tpdc-dpa linker embedded in a polymer matrix, a long lifetime of 199 ms was measured. In the MOF, a decrease down to 180 μ s was observed, which was attributed to either the coordination

interaction between the carboxylic acid and the Zr ions or to interlinker interactions. The QY was measured to be 30% in inert atmosphere. In-air quenching by O₂ reduced the QY to 18% in air (as triplet emission is quenched by O₂). For the future, fabrication of MOF coatings with TADF features offers an exciting prospect toward OLED applications.

In another example, guest-based emission in a SURMOF thin film was explored by Howard and co-workers. In this work, an alternative strategy to enhance fluorescence from the TPE chromophores (described in Section 3.1) was developed. A chromophore with a TPE core was loaded as a guest into a porous MOF thin film so that the phenyl ring rotations were restricted, resulting in a fluorescence quantum yield of \approx 50%. Moreover, the emissive regions could be patterned by employing inkjet printing.^[65]

3.3. Photoexcitation of Linker–Guest or Linker–Linker Coupled Electronic States

3.3.1. Emissive Electronic States

The distances between constituents of a MOF, that is, linkers and nodes, and between these framework components and

embedded guests are well defined, as MOFs are crystalline materials. As a result, their electronic interactions can be computed in a straightforward fashion. This fact is particularly important when it comes to the electronic coupling of chromophores, leading to the formation of electronic states extending over more than a single chromophore. Photoinduced population of such delocalized electronic states can have the following consequences: (a) excited-state dimer and complex formation, (b) excited-state charge transfer (CT), and (c) photoinduced charge separation.

While excimer formation can also occur in homonuclear dimers, for the latter two cases, heterodimers formed by pairing two monomers with different electron affinity is required. Typically, a low-electron-affinity chromophore serves as donor and a second one with high electron affinity serves as acceptor. Each of the three cases has been realized within MOFs and will be discussed next.

Among the reported excimer states in MOF structures, a zirconium-based naphthalenedicarboxylate (NDC) MOF (Zr-NDC) was studied in detail.^[66] The photophysical characterizations were carried out for suspensions of MOF powder in solvent like tetrahydrofuran (THF). An inter-NDC distance (closest C–C distance) of ≈ 4 Å resulted in a broad, featureless excimer emission at ≈ 450 nm upon excitation at 371 nm. Using time-resolved fluorescence spectroscopy, the excimer formation time was determined to be 490–850 ps, and the excimer lifetime was found to be 13–15 ns. Interestingly, using femtosecond spectroscopy, the interparticle excimer formation time was also determined to be ≈ 5 ps, much shorter than that of the intraparticle excimer formation time.

A well-known example of a heterodimer yielding to the formation of CT complexes is the pair tetrathiofulvalene (TTF)/tetracyanonquinodimethane (TCNQ).^[67] TTF/TCNQ dimers display strong redshifted absorption, as the newly formed dimeric electronic states, which can formally be described as $D^{+\delta}-A^{-\delta}$ ($\delta \leq 1$), are substantially stabilized relative to the LUMOs of the individual monomers. The corresponding excited state thus can be viewed as an intermediate step toward complete charge separation (see discussion next).

In 2007, Kitagawa et al. reported an anthracene-based 3D MOF, into which strong electron donors, e.g., aromatic amines and substituted anilines, were loaded as guests.^[24] Strong coupling between the electron donor guests and the electron acceptor anthracene linkers yielded bright green fluorescence with ten times enhanced fluorescence quantum yield compared to that of the pristine host framework. A similar host-guest CT complex was described by Allendorf and co-workers to form in a naphthalene-based MOF, in which different solvents acted as a charge donor.^[68] Zaworotko and co-workers also reported pyrene:4,4'-bipyridine exciplex in a coordination polymer structure.^[69] A molecular-decoding phenomenon was investigated in an interpenetrated, flexible, pillared-layer MOF ($[\text{Zn}_2(\text{bdc})_2(\text{dpNDI})_n]$; bdc = 1,4-benzenedicarboxylate; dpNDI = *N,N'*-di(4-pyridyl)-1,4,5,8-naphthalenediimide) containing an electron-accepting pillar chromophore naphthalenediimide by Kitagawa and co-workers (Figure 9a,b).^[70] The molecular decoding was achieved by the tunable fluorescence of the host-guest CT states, where guests were the aromatic solvent molecules (Figure 9a). The very specific pores created by the

interpenetration of two types of MOFs helped to encapsulate different aromatic guest molecules of variable electron affinities. The different spatial geometry of the host-guest complexes and variable electronic affinities of the guests resulted in a specific CT emission, and hence guest molecules were decoded by emission color. The specific nature of the CT states was further studied later, in 2014, providing details of the dynamic excited-state processes involving exciplex and CT formation (Figure 9c).^[71] Another decoding phenomena, presented as the recognition of aromatic amines through specific host-guest CT complexation, was described in a later year by Maji and co-workers.^[72] The CT emission in that porous, flexible coordination polymer, having host chromophore 1,10-phenanthroline (electron acceptor) and guest aromatic amines (electron donor), was unique (Figure 9d,e), since the CT emission intensity and lifetime were amplified by the efficient energy transfer from the second host linker (2,6-naphthalene dicarboxylate). Such an energy transfer process was feasible because of the preassociated nature of the CT state and the optimal spatial geometry of the energy donor and acceptor. The crystalline coordination pocket showed a tunable CT emission for different aromatic amines, resulting in an excellent amine-recognition material.

While the above-mentioned CT emissive states resulted from intermolecular interactions, also intramolecular charge transfer (ICT) emission in 2D coordination nanosheets was explored by Nishihara and co-workers.^[73] In this case, a new linker 1,3,5-tris[4-(4'-2,2':6',2''-terpyridyl)phenyl]benzene was coordinated to Zn(II) ions to yield a 2D crystalline structure. The fluorescence observed for this layered material was assigned to ICT from triphenyl benzene to Zn(II) coordinated terpyridine part. Such linkers containing a donor as well as an acceptor provide an interesting method to explore bright ICT fluorescence in MOFs.

3.3.2. Photoconductive Electronic State

An interesting next step after the photoinduced occupation of a CT state is the complete dissociation of the corresponding exciton in a spatially separated electron and a hole. Next, we will discuss two examples: linker-linker^[74] and linker-guest interactions.^[75] In the first case, a naphthalenediimide linker-based Co(II)-MOF was studied.^[74] Since in this case the inter-NDI distances are too large to allow for a direct coupling (>0.9 nm), the position of the absorption bands and the interesting redox behavior suggested a metal-to-ligand (or node-to-linker) charge transfer mechanism. Photoexcitation at ≈ 510 nm caused a strong photocurrent response, attributed to the photoexcited electrons and holes. Also, for a number of porphyrin-based MOF structures, a strong photocurrent response was recorded.^[76] In the crystalline MOF structure, the porphyrin linkers are close packed, and the rather small distance between the aromatic cores of only ≈ 0.6 nm facilitates the delocalization of the photoexcitation energy. In this particular case, due to the large library of possible porphyrin linkers with variable light absorption extinction and π -electron delocalization, a series of MOF structures fabricated as thin films (SURMOF) was possible. Recent studies on the isostructural porphyrin MOF thin films also revealed the existence of indirect bandgap

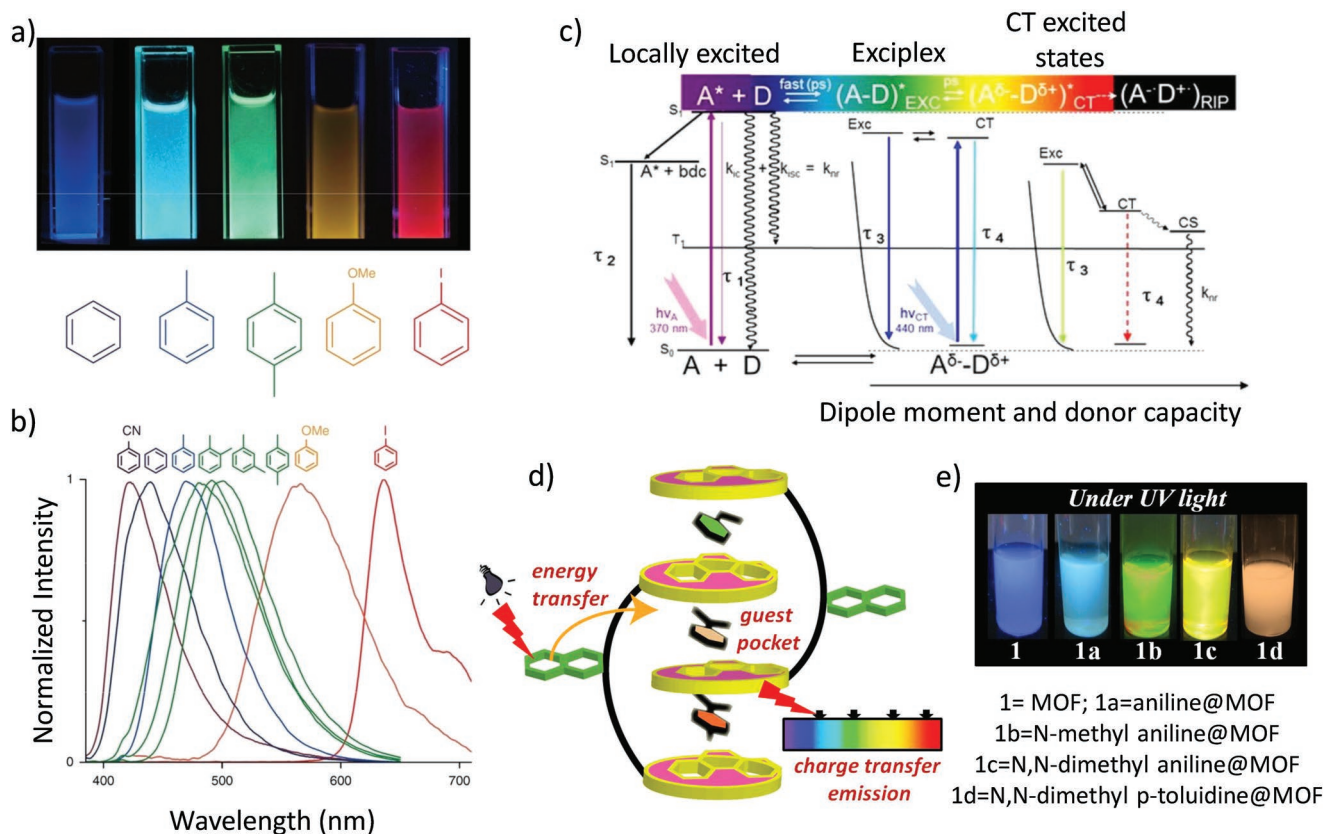


Figure 9. Molecular decoding by $Zn_2(bdc)_2(dpNDI)$. a) Photograph of $Zn_2(bdc)_2(dpNDI)$ MOF dispersed in different aromatic solvents under UV-light illumination. b) Emission spectra of the MOF recorded in different aromatic solvents. a,b) Reproduced with permission.^[70] Copyright 2011, Springer Nature. c) Possible photoexcited states of aromatic guest@MOF. Reproduced with permission.^[71] Copyright 2012, American Chemical Society. d,e) Molecular recognition by flexible supramolecular pocket. d) A schematic showing the supramolecular pocket for guest accommodation and related photophysical process. e) Photograph of the MOF dispersed in different aromatic solvents under UV-light illumination. d,e) Reproduced with permission.^[72] Copyright 2014, Wiley-VCH.

characteristics,^[77] and hence such materials create a large scope for photoresponsive optoelectronic materials based on MOF. Another type of photocurrent-responsive MOF with ICT characteristics (see Section 3.3.1) was demonstrated by Nishihara and co-workers.^[78] Using a bis(dipyrrinato)Zn(II) complex as a basic photofunctional unit, a 2D MOF was constructed, which exhibited a large photocurrent efficiency. It is worth mentioning that the 2D MOFs were deposited in the form of thin films by employing the Langmuir–Schäfer method. The photocurrent measurements were carried out by employing transparent conducting substrates. This example once more demonstrates the advantage monolithic thin films for reliably measuring photophysical properties of chromophoric MOF-based materials; the next example reiterates his fact.

More recently, a host–guest porphyrinic MOF thin film showing pronounced photoconductivity was reported.^[75] Here, a donor–acceptor pair was formed by loading fullerenes (C_{60}) into the pores of the MOF. Since integrating C_{60} into the MOF pores was found to be inefficient using impregnation methods (e.g., immersion of MOF powder or MOF thin films into C_{60} solutions), an lbl fabrication method was employed to fabricate this C_{60} @porphyrin SURMOF, as shown schematically in **Figure 10a**. The conductivity of the C_{60} -encapsulated porphyrin MOF increased to $1.3 \times 10^{-7} \text{ S m}^{-1}$ compared to that of the

empty porphyrin MOF, $1.5 \times 10^{-11} \text{ S m}^{-1}$ (Figure 10c). Upon photoexcitation, a pronounced enhancement of conductivity (two orders of magnitude) was observed (Figure 10b). Apart from these two examples, there are reports on photoinduced CT formation based on host–guest interaction in a powder MOF structure;^[79] however, the photoresponsive conductivity was not explored.

3.4. Energy Transfer: Linker–Linker or Linker–Guest

3.4.1. Singlet Energy Transfer

When two chromophores show a spectral overlap, that is, a regime of photon energies where both emission from the donor (D) and absorption by the acceptor (A) can occur, energy can be transferred from D to A by Förster resonance energy transfer (FRET). The efficiency (E) of this process is governed by the interchromophore distance r ($E \sim 1/r^6$), as well as the relative orientation of the transition dipole moments. In the case of MOFs, fixing the D and A chromophores at well-defined positions of the MOF lattice yields an excellent model system to study FRET processes,^[32] as demonstrated nicely for a strut-to-strut energy transfer process by Hupp and co-workers.^[80] A coassembly of

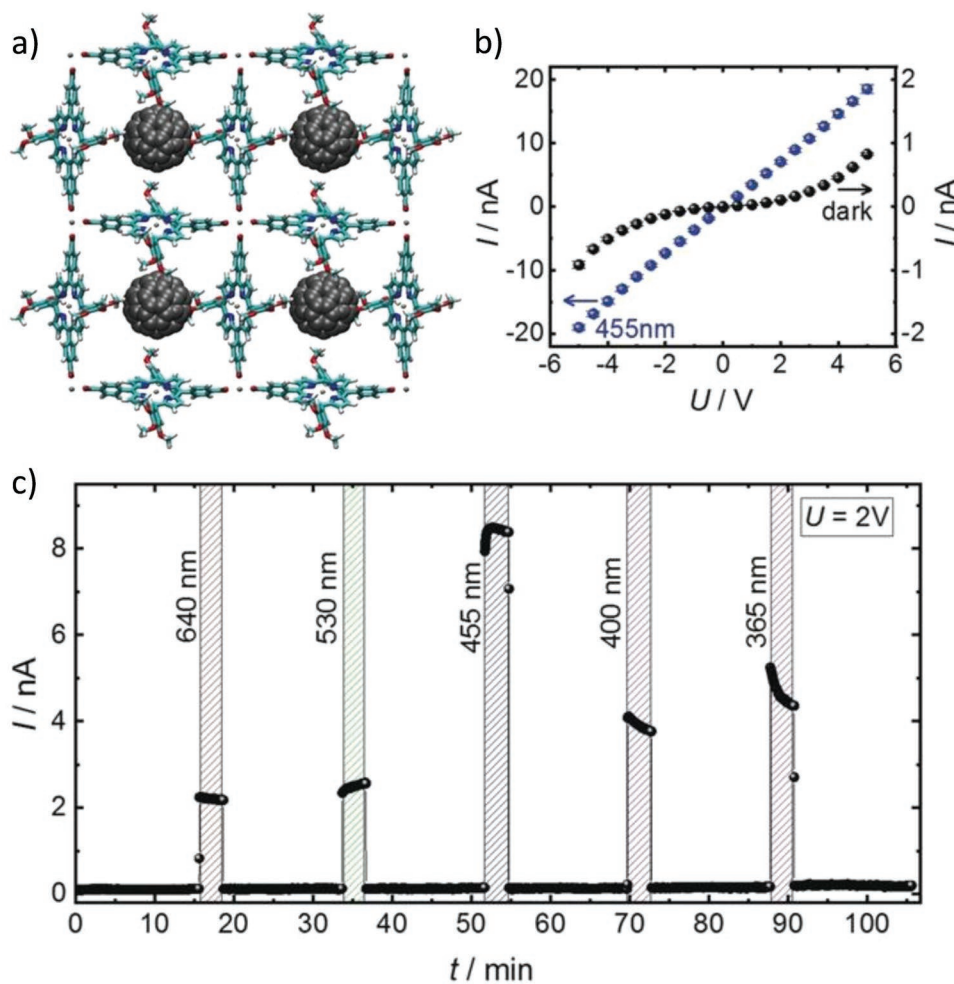


Figure 10. Photoconductivity in a MOF thin film. a) Simulated structure of $C_{60}@Zn-TPP$ MOF. b) DC current at a voltage of 2 V measured for $C_{60}@Zn-TPP$ MOF under different wavelengths of light illumination. c) Current–voltage curve of $C_{60}@Zn-TPP$ MOF in the dark (black spheres) and under irradiation with 455 nm (blue spheres). a–c) Reproduced with permission.^[75] Copyright 2019, Wiley-VCH.

boron dipyrromethene (donor) and zinc-metalated porphyrin (acceptor), in the form of a pillared-layer Zn-based MOF, resulted in an efficient D-to-A energy transfer. The perfect spectral overlap and defined geometry (well-defined distance and relative orientation of D and A) yielded a very efficient FRET process.

Using the linker–guest FRET process, it is also possible to estimate the excitation energy diffusion path. Hupp and co-workers reported a zinc-metalated porphyrin-based MOF, in which the porphyrin linkers acted as pillar linkers.^[81] As an energy acceptor, a pyridyl-ferrocene chromophore was used which can bind to the porphyrin core-Zn(II) through the pyridyl group. A fluorescence quenching experiment, analyzed by Stern–Volmer plot, suggested that the photoexcitation energy in the Zn-porphyrin can migrate in a specific direction anisotropically over 45 Zn-porphyrin chromophores within its lifetime. Such high mobility of the excited-state energy and determination of the transport is unique and could be possible due to the well-defined lattice parameters of the MOF structure. In another example, Lin and co-workers characterized the nature of excitation energy transport by the similar host–guest FRET process (Figure 11).^[82] In this example, a new

MOF was synthesized by connecting a truxene-tribenzoate-based linker (truxene-L) with a $Zn_{10}(\mu_4-O)_4(\text{carboxylate})_{12}$ secondary building unit node. The truxene-L acted as the energy donor, and the guest acceptor was coumerin dye (Figure 11a,b). By encapsulating different concentrations of coumerin dye, the diffusivities of the truxene-L excitons in the frameworks were determined to be 1.8×10^{-2} and $2.3 \times 10^{-2} \text{ cm}^2 \text{ s}^{-1}$, which correspond to the diffusion distances of 43 and 48 nm within their lifetimes, respectively. To explain such transport, a “through space” energy jumping beyond the nearest neighbor model was postulated, and such a long-distance jump accounted for up to 67% of the energy transfer rates (Figure 11c). This study gave clear insight into the singlet exciton diffusion path.

In another example of strut-to-strut energy transport within MOFs, a SURMOF-2 structure^[83] built with anthracenedibenzoic acid (ADB) linkers (Zn-ADB) was investigated.^[84] In this structure, the ADB linkers were arranged in an anisotropic fashion along the [010] crystallographic direction, that is, perpendicular to the substrate plane, with an inter-ADB distance of $\approx 0.6 \text{ nm}$ (Figure 12a). Interestingly, a detailed time-resolved analysis revealed that illuminating with light yielded two

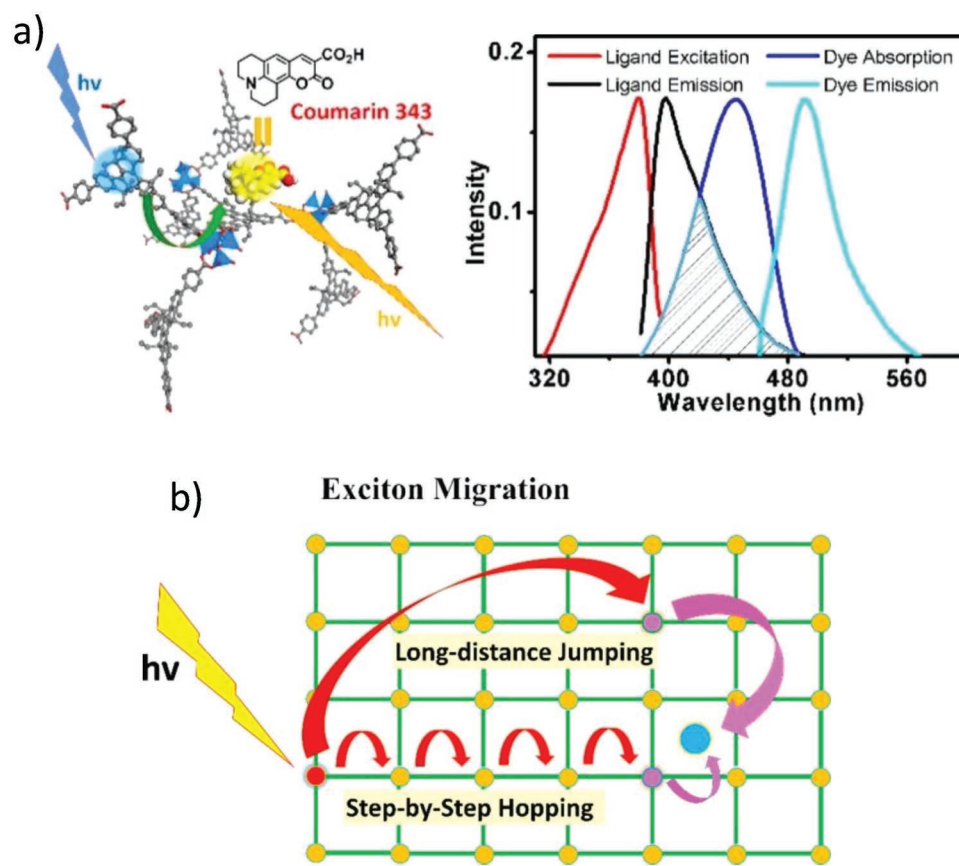


Figure 11. a) The energy transfer path in the coumarin-encapsulated truxene-L-based MOF. b) Spectral overlap of the MOF linker (donor) and coumerin dye (acceptor). c) Schematic of the step-by-step and long-distance jumping of the singlet excitation energy in the coumerin encapsulated MOF. a–c) Reproduced with permission.^[82] Copyright 2016, American Chemical Society.

different states: a monomeric ADB* state as well as an excimer ([ADB-ADB]* state). This interesting observation was explained by the local rotational flexibility of the ADB linker within the MOF structure. This flexibility allowed a second relative orientation of adjacent linkers to be realized, where a rotation of the anthracene unit around the C–C bond allowed for a stronger coupling, yielding to the formation of an excimer state.

A fascinating feature of these two different excitations was the difference in the nature of transport. While the monomeric state showed the expected isotropic diffusion, the dimeric excimer state revealed pronounced diffusion anisotropy. These differences were demonstrated by utilizing the specific advantages of the lbl growth scheme. To measure the directionality of the two excited states, first a suitable energy acceptor linker, diketopyrrolopyrrol (DPP), was mixed in the Zn-ADB structure in different amounts to study the energy transport efficiency (Figure 12a). Using an lbl approach, a pristine Zn-ADB layer was further deposited on top of the mixed-linker layer by the heteroepitaxy method to study the exciton transport perpendicular to the substrate plane (Figure 12b). A detailed analysis of the time-resolved fluorescence data revealed that [ADB-ADB]*, or the excimer diffusion radius, is highly directional and proceeds along the [010] crystallographic direction, parallel to the substrate (Figure 12b). These exciton dynamics were consistent with a Monte Carlo simulation carried out using a simplistic model structure.

This approach of MOF-structure positioning as a heterolayer and the crystallographic insight of donor–acceptor geometry are beneficial to estimating the excitation energy transport. Further examples of such strut-to-strut energy transport are rather scarce,^[85] as in most works of intra-MOF FRET processes, linker-to-guest transfers were studied.

In another case, Hupp and co-workers used CdSe/ZnS core–shell quantum dots as the energy donor guest, which can absorb light in the visible region of the solar spectrum, and the host zinc-metalated porphyrin MOF acted as energy acceptor.^[86] Upon photoexcitation of the encapsulated quantum dots, $\approx 80\%$ energy is transported to the zinc-porphyrin center, as revealed by time-resolved fluorescence measurements. Moreover, this process of guest–host energy transport could harvest $>50\%$ more photon energy than the pristine MOF.

In addition to the improvement of light absorption efficiency, the directionality of the excitation energy transport is another important parameter for light-harvesting materials. This issue was addressed in the earlier example of anisotropic energy transport in a Zn-ADB MOF thin film.^[84] In this regard, Hupp and co-workers also provided a strategy to guide excitation energy in a unidirectional fashion.^[87] They used a pillared-layer Zn-MOF type structure, in which the pillars (pyridyl end group) are perylenediimides (PDIs), and this structure is epitaxially grown on a substrate such that the PDIs are assembled

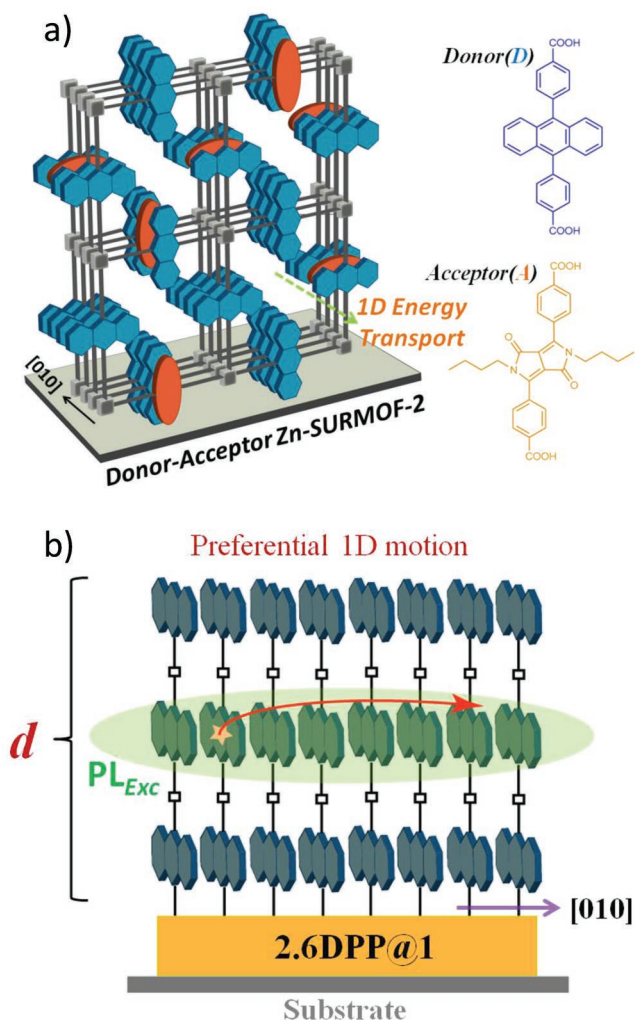


Figure 12. a) Schematic drawing of the donor–acceptor Zn-SURMOF-2 structure showing the preferred exciton diffusion path along the (010) direction. b) Schematic drawing of a heteroepitaxial Zn-SURMOF-2 structure in which the preferential motion of exciton (PL_{Exc}) is shown. a,b) Reproduced under the terms of the CC-BY Creative Commons Attribution 4.0 International License (<http://creativecommons.org/licenses/by/4.0/>).^[84] Copyright 2018, The Authors, published by Springer Nature.

orthogonal to the substrate plane (the orientation was investigated by polarization-dependent absorption). Using lbl method, an energy donor $PDICl_4$ and energy acceptor $PDIOPh_2$ were deposited as the bottom and top layer of a heterolayer structure. On top of this bilayer structure, another energy acceptor, squaraine dye (S1), was deposited so that, upon light absorption by the $PDICl_4$ layer, the excitation energy can be transported to S1 in a direction orthogonal to the substrate plane. In this structure, the vertical alignment of the PDI transition dipoles is the important feature that helps to transport the excitation energy efficiently. Upon photoexcitation of the MOF, only the emission corresponding to S1 was observed, which indicated that the photoexcitation energy of $PDICl_4$ is being transported to S1 via $PDOOPh_2$.

These key concepts of excitation energy dynamics in crystalline MOF structures, as revealed by the linker–guest or

guest–linker FRET process, also have other implications, such as boosting the energy transport,^[88] color tunability, sensing, etc. Hence, a rather large number of studies have been devoted to FRET processes involving a host(linker)–guest.^[89] Encapsulation of the guest chromophore having a partial spectral overlap with the energy donor resulted in dual emission due to incomplete/inefficient energy transfer, and the tuning of this donor–acceptor emission intensity ratio was used for tunable emission and sensing purposes.

3.4.2. Triplet Energy Transfer: Photon Upconversion

Whereas singlet exciton transfer occurs mainly via FRET processes, the transport of triplet excitons requires a Dexter transfer mechanism. Since this type of transport is highly relevant for materials where singlet–triplet conversion is likely, and since triplets are of pronounced interest with regard to photon upconversion via triplet–triplet annihilation, triplet transport has been studied in a number of cases.^[90] The first demonstration (note that an earlier paper by Kimizuka and co-workers^[91] was later withdrawn^[92]) was reported by Howard and co-workers for a donor–acceptor–donor hetero-trilayer, again fabricated using the lbl method (Figure 13).^[90a] The center layer was a Pd-porphyrin SURMOF, which was efficient in light absorption and subsequent singlet–triplet conversion. The top and bottom layer were fabricated from anthracenedibenzoate (ADB), which shows a high efficiency for triplet–triplet annihilation and the subsequent emission of upconverted photons (Figure 13c). It was demonstrated that, in this unique trilayer structure, the Dexter energy transfer (triplet–triplet annihilation) process can be realized efficiently across two organic–organic heterojunctions separating the top and bottom layer from the center layer. The upconversion threshold was found to be about 1 mW cm^{-2} . A later study on the triplet exciton diffusion of the Pd(II) metalated porphyrin linker-based SURMOF revealed its 1D diffusive nature.^[93] A detailed analysis of data from transient absorption spectroscopy revealed that the triplet states of Pd(II)-porphyrin are extremely mobile and exhibit an extraordinarily large transfer rate of 10^{10} s^{-1} . This value corresponds to triplet diffusion lengths on the order of several micrometers for ideal systems. In the experiments, this value was found to be limited to $\approx 100 \text{ nm}$, which is attributed to the crystalline domain size within the SURMOF.

In another study of the upconversion process, a perylene-based MOF thin film was used as an emitter and Pt-octaethylporphyrin was used as a triplet sensitizer.^[90b] The MOF structure was deposited on a TiO_2 surface, while the sensitizer was in an acetonitrile solution of $[Co(bpy)_3]^{2+/3+}$. Using this upconversion process, a significant enhancement of the photocurrent was realized.

4. Photoswitchable MOFs from Photochromic Molecules

Electronic transitions induced by light absorption change the properties of a chromophore. With transient absorption spectroscopy, it can be demonstrated that, during the lifetime of the

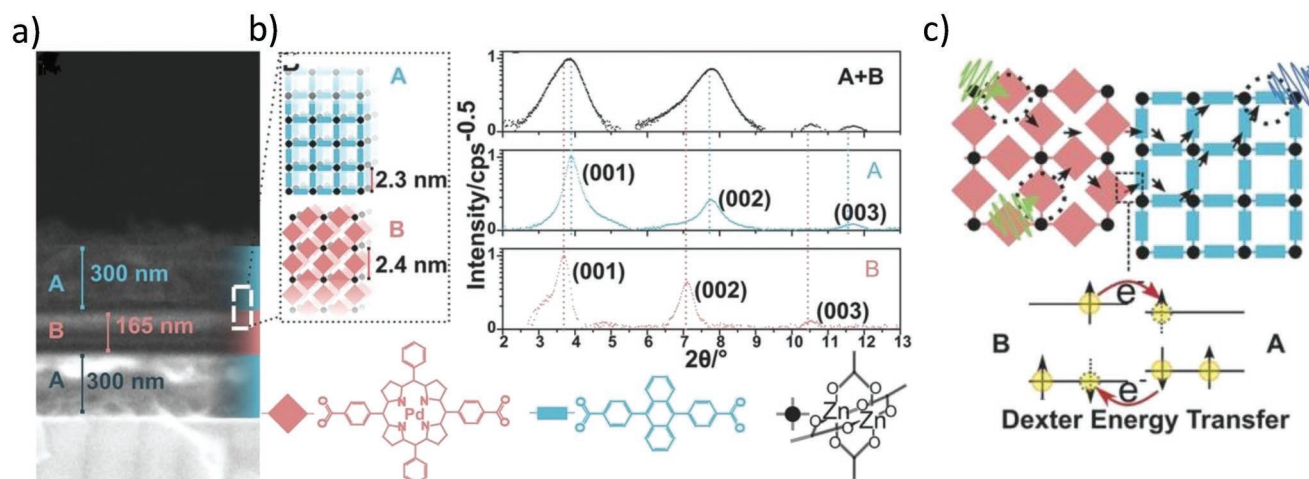


Figure 13. a) A cross-section scanning electron microscopy image of a trilayer heteroepitaxial SURMOF-2 constructed of Pd-porphyrin and anthracene-dibenzoate linkers. b) Out-of-plane XRD data of the heterolayer and pristine SURMOFs. c) A schematic of the Dexter energy transfer at the organic-organic interface of the heterolayer MOF. a–c) Reproduced with permission.^[90a] Copyright 2016, Wiley-VCH.

excitation, the color and absorption spectrum of photochromic molecules are modified. For most molecules, after deexcitation, the molecule returns to its original ground state. For several chemical compounds, however, a different scenario is observed in which the absorbed photon energy is sufficient for a transition to a different conformer, or even for dissociation. The first case, a transition to a different conformer, is often reversible, with the back transition either initiated by thermal energy or again by illumination with light of a different wavelength. Figure 2 shows a few samples of such compounds, which can undergo light-induced *trans*–*cis* and ring-opening/closing isomerizations: azobenzene (AB), spiropyran (SP), and MC, as well as diarylethene (DAE). While these isomerizations can be observed for the free molecule (e.g., in gas-phase and molecular beam experiments^[94]), they are often sterically hindered in the solid state. Thus, it is a major challenge to fabricate materials where the structure changes caused by light absorption in a single molecule can be multiplied to yield changes in the macroscopic material properties.^[95]

The integration of photochromic molecules in solid materials has been made possible in selected cases by creating solid solutions or by directly integrating them into the molecular backbone. Trial-and-error is usually needed to find systems where this approach is successful. Although such materials impressively demonstrate the potential of photoswitchable materials,^[96] the lack of crystallinity makes a rational approach to the design and control of such materials difficult. Moreover, the relatively low density of photoswitches in the material also limits their performance. These limitations can be overcome by using a MOF-based approach, in which photochromic molecules are functionalized to yield di- or higher topic linkers for MOF construction or are loaded into the MOF pores.

The first report on photoinduced changes in a MOF material fabricated from photochromic linkers was on CAU-5, published by Stock and co-workers in 2011.^[97] They described a MOF fabricated from linker molecules with AB side groups. Later, these authors and also Zhou and co-workers demonstrated the light-induced *trans*–*cis* AB isomerization in MOF pores,

which also caused changes in the adsorption capacity of these porous solids.^[98] Sparked by this groundbreaking work, many groups incorporated photoswitchable molecular components in the MOF structure and investigated the photoresponse of the MOF material. Note that MOFs with moieties that are principally photoswitchable have been described before; however, the response toward light was not investigated (e.g., ref. [99]).

The majority of photoswitchable MOFs reported so far was based on AB, followed by DAE components, while only a small number of publications focused on spiropyran (SP) photoswitches (Table 1). Generally, the incorporation of photoswitchable molecules in the MOF material is possible either by simple loading of the photochromic moieties as guests into the pores (Section 4.1.1) or by using linkers containing photoswitchable groups. In the latter case, the photoswitchable group can be either contained in the backbone of the MOF scaffold (Section 4.1.3), or it can be attached to the linkers as a side group (Section 4.1.2, Figure 14). While the MOF lattice typically is not affected by the isomerization of the photoswitch as a pendant group, structural changes are expected when the photoswitchable molecule is incorporated in the backbone of the MOF. In addition to common photoswitches, more complex photoresponsive molecules were incorporated in MOF pores, such as overcrowded alkene molecular motor molecules.^[100] In Section 3.2, we discuss various studies focusing on the photo-modulation of the MOF material properties as a result of the isomerization of the photochromic molecule, ranging from the switching of the color to the remote control of the electronic and magnetic properties. Section 3.3 discusses the control of the host–guest interaction in nanoporous MOFs with photochromic moieties. This allows the switching of the key characteristics of most MOFs, like the adsorption and diffusion properties as well as the proton conduction and catalytic properties.

Due to many structural, chemical, and conceptual similarities with MOFs, photoswitchable COFs and porous organic frameworks (PAFs) are considered here. Since this is a rapidly developing field, a number of review articles are available on photoswitchable MOFs.^[101] Here, we mainly focus on the

Table 1. An overview of reports on photoswitchable MOFs, either in the form of powders or thin films. In this selection, the first publications and the publications with the most impressive switching effects were considered.

Switching of...	MOF material name	Switchable moiety	Result	Ref.	Comment
color	UBMOF-1	DAE	Opened-to-closed: Switching color from transparent white to red/brown	[118b]	
	DMOF3	DAE	Opened-to-closed: Switching color from transparent brown to dark brown	[125]	
	SP@JUC-120	SP	SP-to-MC: Switching color from white to violet	[109c]	Also fluorescence switching. Inverse photochromism
uptake	Cr-MIL-101-Azo	AB	<i>trans-to-cis</i> : CH ₄ uptake increases by ≈50%	[98a]	
	PCN-123 (MOF-5-Azo)	AB	<i>trans-to-cis</i> : CO ₂ uptake decreases by 27%	[98b]	Uptake decreases by another 27% after <i>trans-cis</i> switching.
	PAF-37	AB	<i>trans-to-cis</i> : CO ₂ uptake increases by 12%	[144]	
	UCBZ-1, UCBZ-2, UCBZ-3, and UCBZ-4	AB	<i>trans-to-cis</i> : CO ₂ uptake increases by up to 29%	[142b]	Different numbers of photoswitches per pore
	Amine@UiO-66-Azo	AB	<i>trans-to-cis</i> : CO ₂ uptake decreases by 31%	[148]	CO ₂ affinity of the MOF increases by amine embedment.
	Cu ₂ (DCam) ₂ (AzoBiPyB) SURMOF	AB	<i>trans-to-cis</i> : Switches the enantioselective adsorption ratio of (<i>R</i>)- and (<i>S</i>)-phenylethanol from 2.9 to 1.2	[150]	
	Zn ₂ (BDC) ₂ (DAE-BiPy)	DAE	Opened-to-closed: CO ₂ uptake decreases by 20%	[126]	
	DMOF	DAE	Opened-to-closed: CO ₂ uptake quadruples	[147c]	
	ECUT-30	AB+DAE	UV irradiation (AB <i>trans-to-cis</i> and/or DAE <i>open-to-closed</i>) decreases CO ₂ uptake and increases C ₂ H ₂ :CO ₂ adsorption selectivity estimated by IAST by 108%.	[147a]	Two kinds of photoswitches
diffusion	MOF-808-SP	SP	SP-to-MC: CO ₂ uptake increases by 17%	[111]	SP incorporated by PSM
	Cu ₂ (AzoBPDC) ₂ (BiPy) SURMOF	AB	<i>trans-to-cis</i> : Butanediol diffusion coefficient decreases by factor 15	[121]	Used for remote-controlled release from two-layered-SURMOF
	UiO-68-Azo	AB	<i>trans-to-cis</i> : CO ₂ uptake rate/diffusion coefficient decreases	[143]	
release	IRMOF-74-III-Azo	AB	Irradiation with 408 nm, permanent <i>trans-cis</i> toggle: Release of propidium iodide dye	[151]	
	UiO-68-Azo with cyclodextrin capping	AB	<i>trans-to-cis</i> : Cyclodextrin capping detaches, releases the rhodamine B molecules from the MOF pores	[123]	
	UiO-AZB	AB	<i>trans-to-cis</i> : MOF degradation and release of Nile red	[103]	AB in MOF backbone
	UiO-68-FAzo	Fluorinated AB	<i>trans-to-cis</i> : Release of pyrenecarboxylic acid accelerated	[122]	Core-shell structure
membrane separation	Cu ₂ (AzoBPDC) ₂ (AzoBiPyB) SURMOF	AB	<i>trans-to-cis</i> : Permeance of CO ₂ decreases and H ₂ :CO ₂ separation factor increases from 3 to 8	[104]	Tuning <i>trans-cis</i> ratio steplessly tunes separation factor.

Table 1. Continued.

Switching of...	MOF material name	Switchable moiety	Result	Ref.	Comment
	Cu ₂ (F ₂ AzoBDC) ₂ (dabco) SURMOF	Fluorinated AB	<i>trans-to-cis</i> : Permeance of C ₃ H ₆ increases and H ₂ :C ₃ H ₆ separation factor decreases from 13 to 9	[117b]	No switching effect for H ₂ :CO ₂ separation. <i>trans-to-cis</i> : Butanediol uptake increases by 47%
	AB@UiO-67 membrane	AB	<i>trans-to-cis</i> : Permeance of CO ₂ increases and H ₂ :CO ₂ separation factor decreases from 14 to 10	[107b]	Large effect of AB loading
catalytic properties	SO-PCN	DAE	Opened-to-closed: Singlet oxygen evolution rate decreases	[128]	Energy transfer between DAE and catalytic porphyrin
magnetization	DySc ₂ N@C ₈₀ @UiO-68-Azo	AB	<i>trans-to-cis</i> : Permanent magnetization of metallofullerenes increases	[140]	
proton conductivity	Cu ₂ (F ₂ AzoBDC) ₂ (dabco) SURMOF	fluorinated AB	<i>trans-to-cis</i> : Proton conduction of butanediol and triazol in pores decreases by 35%	[117a]	
electronic conductance	SP@UiO-67 film	SP	SP-to-MC: Conductivity increases by factor 10	[109a]	
	SP-MOF	SP	SP-to-MC: Conductivity increases by 4–30%	[119]	

switchable material properties of the molecular solids resulting from the integration of light-responsive molecules.

4.1. Integration of Photoswitchable Molecules in MOF Materials

4.1.1. Loading Photochromic Guests into MOF Pores

A straightforward method for incorporating photoswitchable molecules in MOFs is by simply embedding them as guest molecules inside the pores (Figure 14a), often denoted as photoswitch@MOF.^[101b] In this approach, the only requirement is that the MOF pores must be large enough to host the photoswitches. In most cases described so far, loading was accomplished by immersing the MOF material in a solution of photoswitches.^[105] Alternatively, loading from the gas phase was also used.^[106] Important parameters for switchable MOFs are the molecular environment in the pores, that is, the guest–host interactions, as well as the degree of loading, that is, the guest–guest interactions. Since the guests are not attached to the framework, the molecules are mobile and may diffuse, potentially resulting in a rather complex situation with many different local structures. They also may eventually leave the pore system again, typically with a very small release rate due to the very low vapor pressure. For SURMOF thin films loaded with AB, it was shown that the photoswitches evaporate from the MOF at room temperature with a time constant of about one year.^[105] Thus, the photoswitch@MOF is sufficiently stable for most experiments.

AB,^[102,105,107] DAE,^[108] and SP^[106,109] molecules were used to implement the photoswitchable properties by the embedment of the photochromes in the pores. In that way, the color^[106,109c] and the adsorption^[105,107a] properties of the material could be modified by illumination.

Photoswitch@MOF materials are also suitable as model systems to characterize the switching process in more detail.

A particular advantage is the fact that the vibrational transitions in MOFs are barely broadened relative to the free linker molecules, resulting in individual, relatively sharp infrared absorption bands. Therefore, unlike most solvents and polymers, MOFs are transparent to infrared light over fairly large regions, allowing for spectroscopic investigations, e.g., in the 650 to 1300 cm⁻¹ regime.^[102] For example, the *trans* azobenzene band at 780 cm⁻¹ as well as the CO-spiro band at 1280 cm⁻¹ of SP were used to quantify the isomer composition at the photostationary state (PSS).^[102,105,109a]

Since the situation of photoswitchable molecules hosted in MOF pores bears some similarities to the solvated situation, Ruschewitz and co-workers used the term “solid solvents” for the host MOFs.^[106] They showed that changes of the MOF pore polarity result in shifts of the absorption spectra of the embedded SP guest molecules, similar to the solvatochromism in (liquid) solvents.

For most photoswitch@MOF cases, the switching of the guest does not change the structure of the host framework. However, Kitagawa and co-workers showed that, for a flexible, guest-responsive MOF powder of type Zn₂(BDC)₂(dabco), the embedment of AB guests resulted in structural changes of the parent MOF. Moreover, the *trans-cis* isomerization of the guest molecule changed the host MOF structure.^[107a] It is noteworthy that no changes were observed upon *trans-cis* switching of a similar photoswitch, 2-phenylazopyridine in the same MOF structure.^[110]

4.1.2. Incorporation of Photochromic Moieties as a Side Group of the MOF Linker

When covalently attaching the molecular photoswitch as pendant or side group to a MOF linker, the steric requirements are less severe. Numerous examples of such functionalized linkers have been reported. For AB, one of the simplest cases

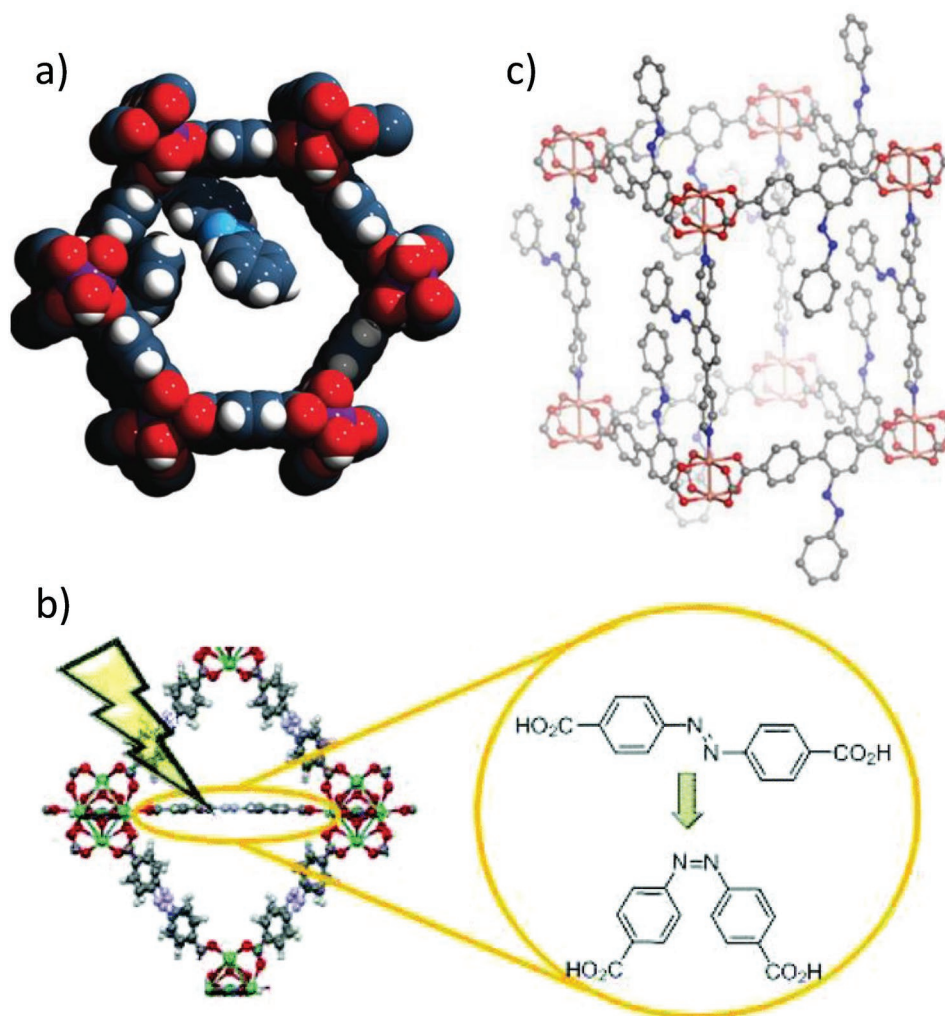


Figure 14. a) A molecular photoswitch can be implemented in the MOF material by simple embedding in the pores, b) by appropriate functionalization and incorporation in the MOF backbone; or c) by appropriate functionalization and incorporation as a side group of the MOF structure. a) Reproduced with permission.^[102] Copyright 2013, American Chemical Society. b) Reproduced with permission.^[103] Copyright 2017, The Royal Society of Chemistry. c) Reproduced under the terms of the CC-BY Creative Commons Attribution 4.0 International License (<http://creativecommons.org/licenses/by/4.0/>).^[104] Copyright 2016, The Authors, published by Springer Nature.

is obtained by functionalizing one of the phenyl groups with two carboxylic acid groups in para position.^[101g] Of interest are also approaches where the entire photoswitch is attached to the linkers after MOF construction by so-called postsynthetic modifications (PSM).^[98a,111]

When attaching photoswitchable side groups to the MOF linker, the pore space needs to be sufficiently large to allow for the conformational transition to occur. For this to be possible, it is not sufficient to only check the initial and final states, as the full path has to be considered. For example, combined experimental and theoretical investigations for MOF thin films of pillared-layer structure—type $\text{Cu}_2(\text{AzoBPDC})_2(\text{BiPy})$ and $\text{Cu}_2(2,6\text{-NDC})_2(\text{AzoBiPy})$ —that is, the Cu analogue and structural isomorph of $\text{Zn}_2(2,6\text{-NDC})_2(\text{AzoBiPy})$, also referred to as CAU-5—showed that slight structural changes can block the photoisomerization.^[112] While the photoisomerization in $\text{Cu}_2(\text{AzoBPDC})_2(\text{BiPy})$ is similar to the isomerization of

the free molecule, the photoisomerization path in $\text{Cu}_2(2,6\text{-NDC})_2(\text{AzoBiPy})$ is sterically hindered, suppressing the *trans-cis* photoswitching, although both the *trans* and the *cis* isomers have sufficient space. Steric hindrance of the photoisomerization was also found for F-Azo-MIL-53(Al), where the light irradiation does not result in *trans-cis* switching but only results in photothermal effects decreasing the adsorption capacity.^[113]

MOFs where the isomerization of the photochromic side group occurs unhindered can serve as valuable model system for a detailed investigation of the isomerization mechanism. By thermal *cis-to-trans* relaxation experiments at different temperatures in vacuum,^[114] as well as in an argon atmosphere or in butanediol,^[115] the relaxation rate and the activation energy were determined in the absence of solvent effects. The corresponding data provided the first reliable experimental activation energy for the activation barrier governing backswitching of azobenzene. The experimentally determined values were in

very good agreement with theoretical predictions for isolated azobenzene molecules.

While many studies use linkers with plain AB side groups, which are switched with UV and visible light, in a few cases linkers were also functionalized with fluorinated AB moieties.^[116] Such compounds are of interest since they allow switching with visible light, thus avoiding UV light.^[113,117]

In addition to AB, DAE^[118] and SP^[111,119] were also incorporated into MOFs as photoswitchable side groups. DAE-MOFs were synthesized from carboxylic acid or pyridine-functionalized DAE linkers. For the fabrication of SP MOFs, the SP side groups were either attached to appropriate linker molecules^[119] or covalently coupled to the MOF struts by postsynthetic modification.^[111]

A number of interesting applications are possible when fabricating MOF materials with more complex architectures, e.g., MOF multi-heterolayers fabricated by lbl techniques^[120] or core-shell particles. So far, such photoswitchable MOF heterostructures have only been prepared with AB side groups. A two-layered photoswitchable SURMOF thin film with a passive container layer at the bottom and a photoswitchable layer on top has been fabricated to serve as a remote-controllable release system.^[121] A powder MOF equivalent, a core-shell MOF with UiO-68 MOF structure, has been prepared by Hecht and co-worker. In this case, the photoswitchable moieties were incorporated by linker exchange in the outer MOF shell.^[122] Wang and co-workers used an Azo-UiO-68 MOF powder with a cyclodextrin capping blocking the pore entrances.^[123]

4.1.3. Incorporation of Photochromic Moieties in the MOF-Linker Backbone

The incorporation of molecular photoswitches in the backbone of a ditopic linker, and thus in the backbone of the corresponding MOF, can be achieved by attaching appropriate coupling units, for instance, two carboxylic acid or pyridyl groups at opposite sides of the molecule (see Figure 14b). Since the incorporation into the MOF scaffold decreases the mobility and reduces the conformational freedom, such integration is particularly suitable for photochromic moieties for which the switching causes only small structural changes, like in the case of DAE.^[124] For most DAE derivatives, the UV-induced ring closing goes along with a slight change in the molecular length (by a few %) without further substantial changes in molecular components. Indeed, MOF materials containing DAE in their backbone showed slight changes in their structure,^[125] adsorption capacity,^[126] selectivity,^[127] and catalytic properties.^[128]

The situation is different when the photoinduced molecular isomerization goes along with large structural changes, like for the *trans-cis* AB isomerization and even more so for the SP-MC isomerization. As a result, the photoisomerization of the molecular switch integrated in the MOF backbone is sterically hindered, leading either to no change at all^[129] or to bond breaking, a decrease of MOF crystallinity, and a general degradation of the framework.^[103,130] Bond breaking and MOF degradation can also be employed as useful feature. Morris and co-workers used the degradation of a UiO-type MOF with AB photoswitches in

the backbone to achieve a UV-light-induced release of Nile red molecules.^[103] Using such linker molecules, the MOF morphology can also be modulated by *trans-cis* switching of the linker molecules before MOF synthesis.^[131]

In a number of works on MOFs with AB units in the backbone, illumination was reported to decrease the uptake of guest molecules, but these works did not clearly address forward and backward switching between the *trans* and *cis* states by UV (*trans-to-cis*) and visible (*cis-to-trans*) light.^[132] Spectroscopic investigations to demonstrate that illumination results in *cis* conformations were not presented. In these uptake studies, after irradiation and the correlated uptake decrease, the uptake amount of the excited state immediately increases back to the pristine state. Such fast transition back to the ground state is not consistent with AB *trans-cis* isomerization, where (unless the AB moieties are functionalized by electron push-pull groups) the *cis* state is metastable with a half-life of many hours to weeks.^[96a] While the particular environment in the MOF pore might, in principle, account for such tremendous deviations from normal behavior in common solvents, a more detailed investigation is required to determine whether the decrease in adsorption capacity might be caused by other effects related to light irradiation, e.g., a local temperature increase. In fact, steric isomerization hindrance and a thermally induced change in the adsorption capacity was reported for MOFs made from linkers with AB side groups^[113] (see also previous section).

4.2. Photoswitching the Properties of MOF Materials

The major goal when incorporating photoswitchable moieties into MOFs is to translate the isomerization of the individual photoactive molecules into changes in the macroscopic properties of these crystalline molecular solids. In recent years, several examples have become available showing that the physical properties of MOF particles of a thin film could be remote controlled by light, including color, fluorescence, electronic structure, and magnetic response. In addition, MOFs are nanoporous materials, and the uptake of guest molecules is a crucial property. Accordingly, photoswitchable MOFs have been used to control the adsorption, diffusion, and (membrane) permeation as well as the proton conduction properties of the guest molecules. In addition, the catalytic properties of MOFs containing photoswitchable groups can be modified by illumination.

4.2.1. Switching Color and Fluorescence

Remote control of MOF color can be achieved by incorporating photochromic molecules with strong differences in the absorption spectrum between the different photoisomers. One of the most popular examples is the SP/MC pair. The SP conformer barely absorbs in the visible range, whereas MC strongly absorbs with an absorption maximum depending on the environment and functionalization. As a result, the corresponding MOF material shows pronounced photochromism. The potential applications of such color-tunable materials range from remote-controllable, switchable windows to displays, and even defect visualization in materials by the use of such MOF

coatings has been envisioned.^[133] Proof-of-principle demonstrations have been reported for SP embedded into the pores of JUC-120 COF^[109c] as well as in MOFs of type MOF-5, MIL-68(In), and MIL-68(Ga).^[106] In all cases, strong photochromic behavior of the MOF material was observed. The SP-MC properties were found to strongly depend on the pore environment, as discussed above. Interestingly, due to the confinement in the polar JUC-120 COF pores, SP was destabilized relative to MC, so that the thermodynamically stable form was the violet MC form that, by irradiation with UV light, could be switched to the colorless SP form (Figure 15a).

Klajn and co-workers incorporated SP as side groups into a COF framework.^[134] In addition to the visible color, the fluorescence intensity could also be switched (Figure 15b). This latter effect employs the bright fluorescence of MC, whereas SP is nonfluorescent.

DAE also shows significant differences in color: the open-ring form is colorless, while the closed-ring form is strongly colored. Benedict and co-workers used a DAE-MOF for investigating the isomerizations and the color changes of the framework material.^[108b,118]

4.2.2. Switching the Electrical Conductivity

The electronic properties of MOFs, which may behave as conductors, semiconductors, or insulators, attract substantial attention with respect to device applications, including chemical sensors, supercapacitors, and batteries.^[135] Accordingly, the remote control of MOF electronic properties is highly interesting with regard to further advances in this field. It is known that single-molecule SP junctions, as well as SP monolayers, show strong changes in electrical conductivity upon SP-MC photoisomerization.^[136]

Inspired by these findings, Garg et al. used UiO-67 MOF films loaded with commercially available nitro-substituted SP to demonstrate light-induced switching of electrical conductivity in a MOF material.^[109a] Upon UV-light-induced SP-to-MC isomerization, reaching a PSS of 70% MC, the conductivity of the material reversibly increased by a factor of 10. Density functional theory (DFT) calculations revealed the origin of the experimentally observed phenomenon. The SP-to-MC isomerization goes along with a decrease in the orbital localization. While the HOMO and LUMO orbitals of SP are localized at the chromene and indolene moiety, respectively, for the MC isomer, both orbitals are

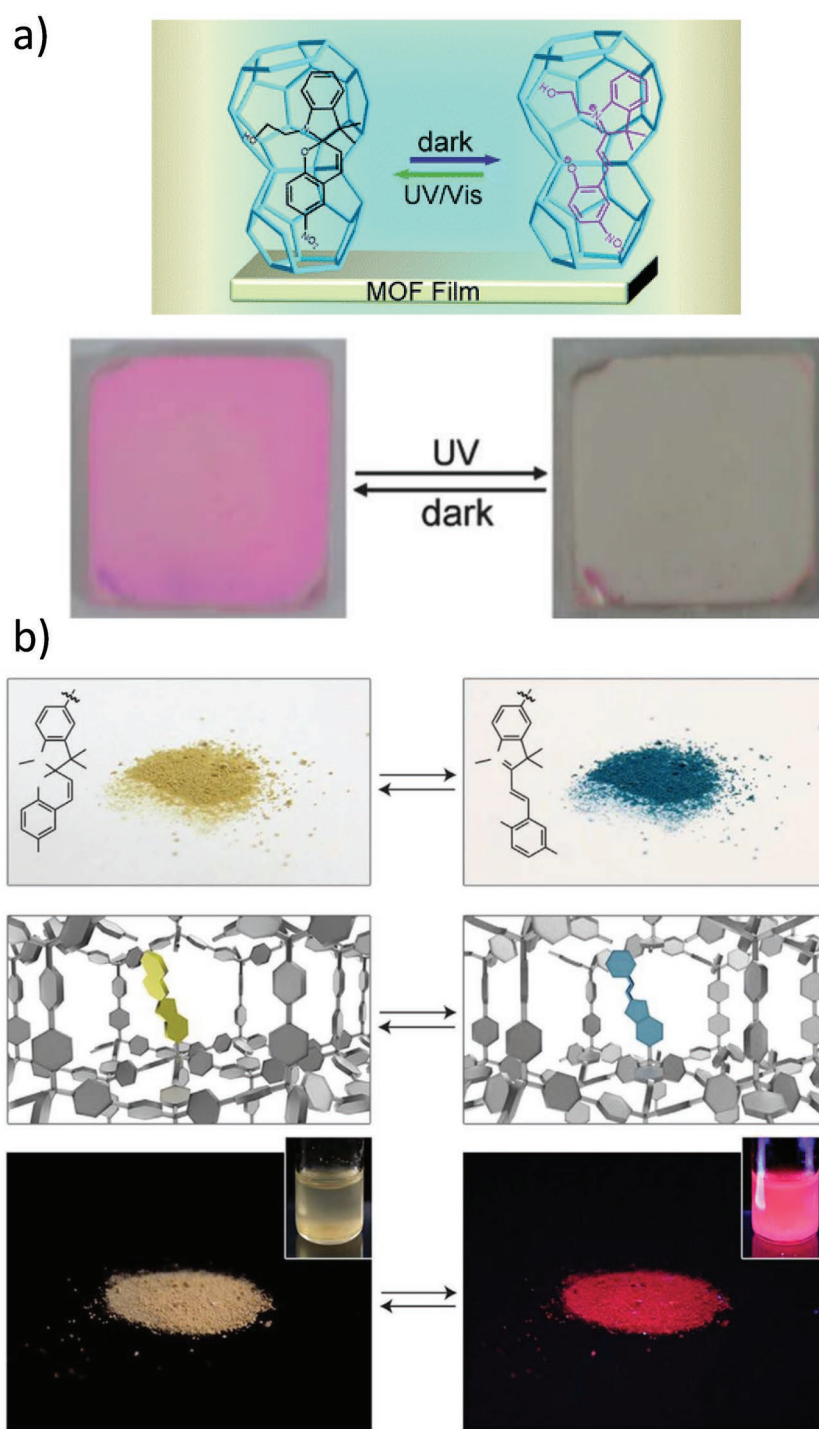


Figure 15. Switching the color and fluorescence of the material. a) Sketch of the SP@JUC-120 COF with SP on the right-hand side and MC on the left. Reproduced with permission.^[109c] Copyright 2012, The Royal Society of Chemistry. Bottom: Photographic images of the SP@JUC-120 COF film with and without UV irradiation. b) Porous aromatic framework with SP side groups. Reproduced with permission.^[134] Copyright 2014, Springer Nature. Top: Visual changes to the framework with SP side groups upon exposure to low-intensity UV light. SP left, MC right. Center: Schematic representation of the framework with efficient isomerization of spiroopyran inside the nanopores. Bottom: Visual changes to the sample in the solid state and in a toluene suspension (insets) as a result of UV irradiation. Images on the left were taken under ambient light. Images on the right were taken in the dark under 365 nm illumination.

delocalized over the entire molecule. In addition to the increase in the electron orbital delocalization, the MC isomer has an ≈ 0.2 nm longer extension, thus decreasing the charge hopping distance and increasing the rate for charge transfer (Figure 16). While the experiments show that the MOF material conduction increases by one order of magnitude upon SP-to-MC isomerization of the randomly distributed molecules in the MOF pores, theoretical calculations predict that a conduction increase of up to four orders of magnitude is possible if the molecules have identical intermolecular distances in the range 1.3–1.5 nm.^[109a]

In a later study, Shustova and co-workers incorporated SP as side groups and investigated the conductance switching.^[119] There, upon SP-to-MC switching, the conduction increased by $\approx 20\%$ for MOF pellets and 4% for a large MOF single crystal. In this proof-of-principle study, the isomer composition at the PSS was not determined. It may be speculated that, due to the strong SP absorption intensities, only the SP molecules in the outer MOF material switches to MC, and the majority remains as SP isomer, resulting in a very small average PSS and a small switching effect.

4.2.3. Switching the Magnetization

The use of functional molecules offers interesting options for studying crystalline MOF assemblies of another class of materials, molecular magnets.^[138] Among the recent research foci were single-molecule magnets, spin-crossover MOFs, and MOFs for magnetic refrigeration.^[139] The remote control of these properties is highly interesting. Wang and co-workers demonstrated that the magnetization of a UiO-68 MOF powder with AB side groups and embedded magnetic metallofullerenes can be controlled by light (Figure 17).^[140] UV-induced *trans*-to-*cis* isomerization of the AB units was found to increase the magnetization of the metallofullerene@MOF system. The authors explained the observed effect by the stronger host-guest interaction, leading to a suppression of the quantum tunneling of magnetism (QTM) effect and increasing the response of the embedded metallofullerene to the external magnetic field.^[140]

4.3. Switching Guest-Host Interaction in Photochromic MOFs

The most important application field of MOFs is gas storage and separation. The uptake of guest molecules into the pores is controlled by host-guest interactions, which are typically complex. These comprise attractive and repulsive interactions based on Coulomb and electric forces, hydrogen bonds, π - π interaction, dipole-dipole, van der Waals forces, etc. Photoisomerization of MOF constituents offers several options to affect these interactions and thus introduce optical control into this important MOF application field.

In the case of MOFs made from linkers with AB side groups, it was found for pillared-layer MOF films of type $\text{Cu}_2(\text{BDC})_2(\text{AzoBiPyB})$ that the effect of the *trans*-*cis* switching on the uptake increased with increasing polarity of the guest molecules.^[141] The experimental data indicated a dipole-dipole, also known as Keesom, interaction between the polar guests and the dipole of AB (see Figure 2). A dominating role of attractive

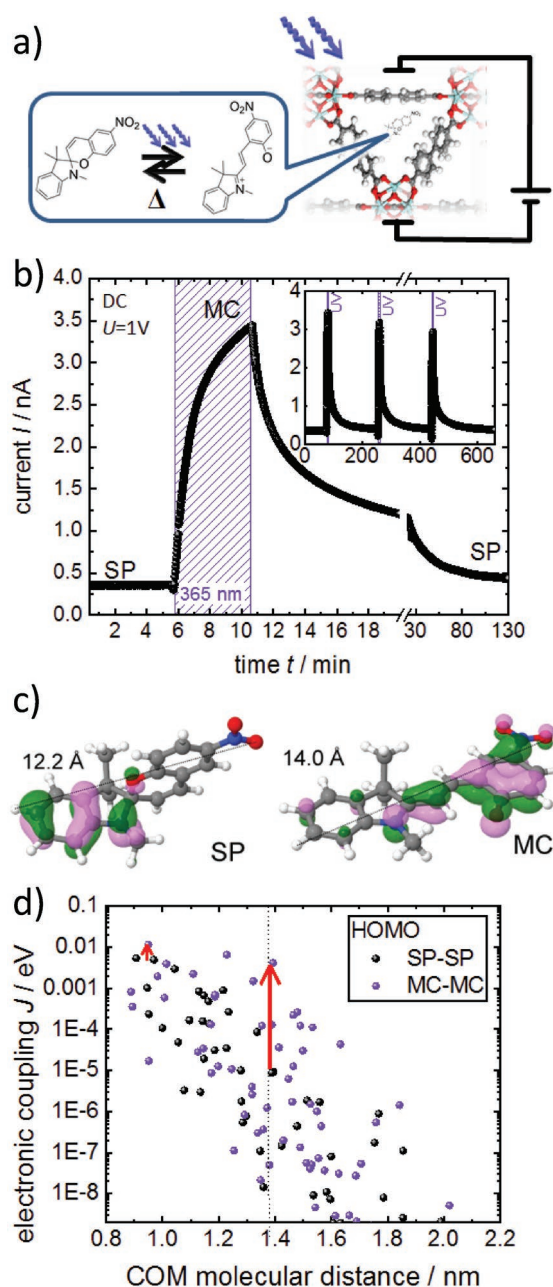


Figure 16. Electronic conductance photoswitching of SP@UiO-67-MOF films. a) Sketch of the UiO-67 MOF with the embedded SP. b) The measured current at a DC voltage of +1 V. The sample was irradiated with 365 nm UV light for 5 min. c) DFT calculations of microscopic parameters with the molecular structure of SP and MC and visualizations of the highest occupied molecular orbital (HOMO). The electronic coupling elements J are between the HOMOs of SP-SP and of MC-MC as a function of their center-of-mass (COM) distance. The electronic conduction in organic materials can be described with Marcus theory,^[137] where the hopping rate (as a measure for the conductivity) is proportional to the square of the electronic coupling elements J between the molecules. The experimentally estimated average distance (1.37 nm) between the molecules is indicated by the dashed line. The red arrows symbolize the SP-to-MC coupling increase for a small COM and for the average COM. Since the coupling at smaller distances is much stronger, these pathways dominate the electron conduction. a–c) Reproduced with permission.^[109a] Copyright 2019, Wiley-VCH.

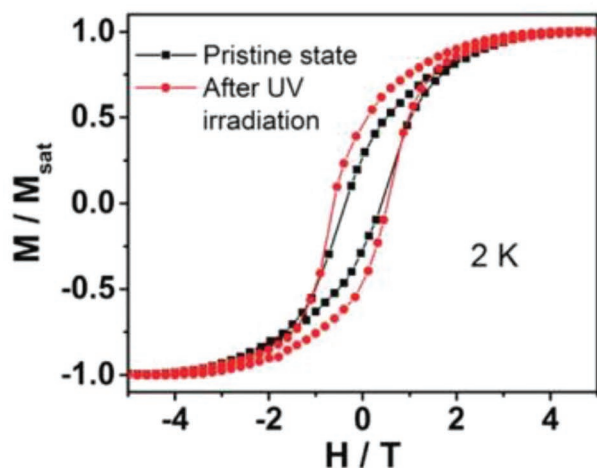
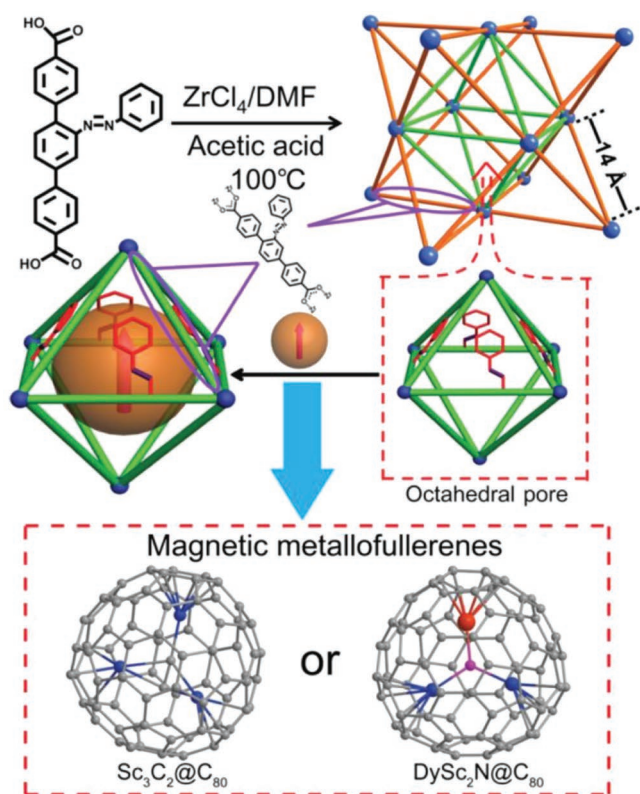


Figure 17. Schematic illustration of the synthesis of the Azo-UiO-68 MOF and construction of metallofullerene@Azo-UiO-68. The schematic structures of $Sc_3C_2@C_{80}$ and $DySc_2N@C_{80}$ metallofullerene are shown in the center (Sc: blue, N: pink, C: gray, and Dy: orange). Bottom: Hysteresis loops for $DySc_2N@C_{80}@Azo-UiO-68$ in the pristine state (black, *trans*) and after irradiation with UV for 30 min (red, *cis*) at 2 K. Reproduced with permission.^[140] Copyright 2018, American Chemical Society.

polar interaction with *cis* AB was also reported for other MOF structures containing linkers with AB side groups.^[104,121,142] Theoretical results confirmed the importance of these electrostatic interactions.^[117a] In an elegant work, Aida and co-workers directly demonstrated optical switching of polarity inside UiO-68-Azo MOFs by embedding polarity-sensitive dye molecules.^[143]

In addition to changes in polarity, steric effects may also matter. For example, the azobenzene side group in one form (usually *cis*) may shield attractive sites for guest adsorption.^[98b,144] Since most MOFs are rather flexible frameworks, with various parts of the framework rotating or wiggling at room temperature, a detailed experimental determination of the shielding effect is challenging. For PCN-123,^[98b] the shielding effect was also investigated by detailed structure calculations.^[145] Switching may also reduce the available pore diameter and window size, thus reducing the diffusion and mass transfer.^[117b]

It should be noted that the effect of photoisomerization in MOFs on the uptake of a given guest is difficult to predict, since various interactions contribute to this effect and general guidelines are lacking. Recently, in a systematic study of uptake experiments with MOF thin films made from a variety of different linkers, Wang et al. demonstrated that increasing the density of AB side groups per volume, rather than the number of AB units per pore, increases *trans-cis* switching effects.^[142a]

For DAE, the situation seems similarly complex, and the observed property changes result from a combination of structural changes and the changed electrostatic interactions.

Since the dipole moment change for SP-MC isomerization is very large and the long MC molecule has a rather flexible structure, it can be assumed that the changes in the polar interaction dominate the switching effects of the guest–host interaction in SP MOFs.

4.3.1. Photoswitching of Uptake and Release of Guest Molecules

While the storage of H_2 and CH_4 possibly finds application in automobile gas tanks, the storage of CO_2 in MOFs might help with the capturing, storing, and sequestering of this greenhouse gas. In this respect, the remote control and photo-switching of the CO_2 adsorption capacity in MOF powders and pellets is envisioned to increase the efficiency and decrease the energy demand during the cycling of these processes. To this end, the switching of the CO_2 adsorption capacity of MOF powders with AB,^[98b,113,125,143,144,146] DAE,^[126,147] and SP^[111] moieties has been investigated.

Zhou and co-workers prepared PCN-123, that is, MOF-5 with additional AB side groups, where the CO_2 uptake is modulated by UV irradiation and by the subsequent thermal relaxation of the AB groups (Figure 18). The uptake decrease upon *trans*-to-*cis* switching is explained by a shielding of the metal centers, which are attractive CO_2 adsorption sites.

Since the affinity of most MOFs toward CO_2 is rather low, Sun and co-workers used an UiO-66 MOF with AB side groups and embedded tetraethylenepentamine to increase the CO_2 affinity.^[148] Similar to a previous study by these authors in mesoporous silica,^[149] due to the attractive interaction between *cis* AB and the amine, the attractive CO_2 adsorption sites were blocked upon photoisomerization. As a result, the adsorption capacity of the MOF material in the *cis* form is significantly decreased upon illumination with UV light.

Kitagawa and co-workers^[126] prepared interpenetrated pillared-layer DAE MOFs and demonstrated structural changes as result of the light-induced ring opening and ring closing. Along with the changes in the MOF structure, the CO_2 adsorption

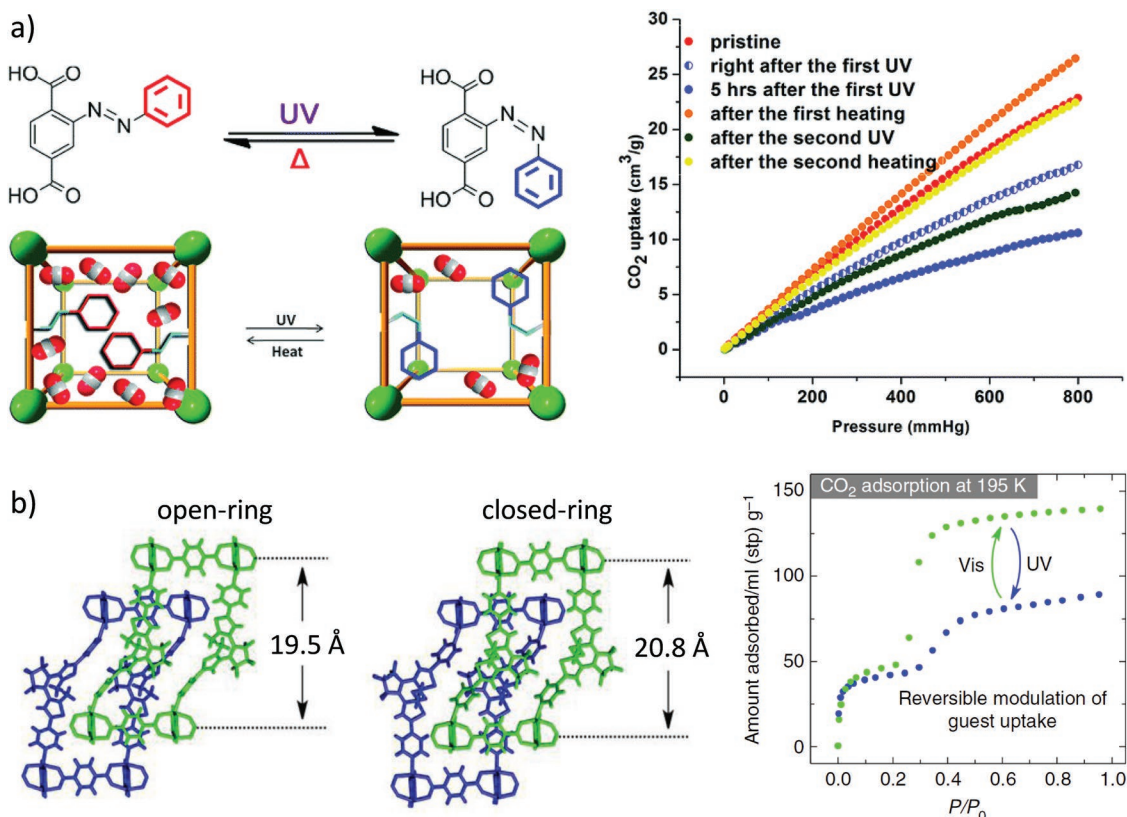


Figure 18. Switching of CO₂ uptake in photoswitchable MOFs. a) MOF with AB side group. Left: *trans*–*cis* isomerization of the ligand of PCN-123 (PCN: porous coordination networks), with a schematic illustration showing the suggested CO₂ uptake in PCN-123 *trans* and PCN-123 *cis*. Right: CO₂ adsorption isotherms (at 295 K) of PCN-123 showing reversible conformational change: pristine sample (red), right after the first UV irradiation (half-filled blue), 5 h after the first UV irradiation (fully filled blue), after the first regeneration process at 60 °C for 20 h in the dark (orange), after the second UV irradiation (green), and after the second regeneration process at 60 °C for 20 h in the dark (yellow). b) DAE MOF. Left: The guest-free, interpenetrated crystal structure in the open-ring and closed-ring form. The MOF lattice distance changes by ≈7%. Right: The highly effective photochemical reaction in the porous crystal realizes a reversible modulation of CO₂ sorption. The CO₂ adsorption isotherms were measured at 195 K. a) Reproduced with permission.^[98b] Copyright 2012, American Chemical Society. b) Reproduced under the terms of the CC-BY Creative Commons Attribution 4.0 International License (<http://creativecommons.org/licenses/by/4.0/>).^[126] Copyright 2017, The Authors, published by Springer Nature.

capacity reversibly decreases by ≈20% upon UV-light irradiation. Guo and co-workers prepared DAE MOFs and showed that the CO₂ adsorption capacity increases by a factor of 4 upon UV-induced ring closing.^[147c] This is the largest on-off ratio for CO₂ uptake reported to date.

Apart from CO₂, the uptake of other gas molecules is also relevant for numerous MOF applications. For instance, the CH₄ uptake in MOFs with AB side groups was photomodulated,^[98a] as well as the C₂H₂ and C₂H₄ adsorption, in DAE MOFs.^[127] SURMOFs with AB side groups were used to modulate the uptake of various vapor molecules, such as ethanol, propanol, butanol, ethanediol, propanediol, and butanediol.^[117a,141,142]

By using MOF materials comprising photoswitchable AB and chiral *D*-camphoric acid (Dcam) components, the enantioselective adsorption was photomodulated in a Cu₂(Dcam)₂(AzoBiPyB) SURMOF.^[150] While the *cis* form shows almost no adsorption selectivity, the adsorption of (*S*)- and (*R*)-phenylethanol in the *trans* form is enantioselective, exhibiting a (*S*) versus (*R*) uptake ratio of about 3.

Optical switching of uptake and release is not limited to the gas phase, since the loading can also be controlled by

photoisomerization in the liquid phase. Yaghi and co-workers demonstrated light-induced release of a propidium dye from an IRMOF-74-III with AB side groups by irradiation with 408 nm light.^[151] This wavelength, which is close to the isosbestic point between the absorption bands of the *trans* and *cis* isomers, simultaneously stimulates the *trans*-to-*cis* and *cis*-to-*trans* isomerization. The authors attributed the release of the embedded molecules to the energy absorption and the toggle motion of the AB groups. Hecht and co-workers used UiO-68-MOFs with a core-shell structure (see above) to demonstrate optical control of uptake and release of pyrenecarboxylic acid in ethanol.^[122]

The remote-controlled release of rhodamine B from an Azo-UiO-MOF powder in water was demonstrated by Wang and co-workers using a cyclodextrin capping at the outer surface of the MOF particles.^[123] Initially, the rhodamine B guest molecules were loaded in the MOF and the subsequently attached cyclodextrin capping enclosed the guests in the pores. By UV-light-induced *trans*–*cis* isomerization, the cyclodextrin capping detached and the guest molecules were released.

4.3.2. Photoswitching of Diffusion Properties

The mass transfer of the guest molecules through the host network of pores is crucial for the most important applications of MOFs, such as gas storage, separation, and catalysis. The diffusivity of embedded moieties is pivotal for efficient performance, e.g., in the context of reactants transport to catalytic active sites or analyte transport to sensory sites. As a result, the diffusion of guest species in MOFs has been intensively investigated.^[153] Not surprisingly, the possibility of controlling transport phenomena via remote optical control is of interest in many contexts.

For diffusion switching, a two-layered SURMOF with a passive pillared-layer SURMOF $\text{Cu}_2(\text{BPDC})_2(\text{BiPy})$ bottom layer and a photoactive top layer of the same MOF backbone structure with additional AB side groups, $\text{Cu}_2(\text{AzoBPDC})_2(\text{BiPy})$, was prepared (Figure 19).^[121] By uptake experiments with butanediol as the probe molecule using a quartz crystal microbalance (QCM),^[153] it was shown that the *trans*-to-*cis* isomerization decreased the butanediol uptake rate by a factor of 15. The uptake by the SURMOF hetero-bilayer is much slower than that by the $\text{Cu}_2(\text{BPDC})_2(\text{BiPy})$ SURMOF bottom layer (see Figure 19b). Thus, it must be concluded that the mass transport resistance in the photoswitchable top layer dominates the overall mass transfer. The transport resistance of this top layer may be described by the permeability k , which correlates to the diffusivity D by $k = D/\delta$, with δ denoting the layer thickness.^[152] On the other hand, the permeability is calculated by $k = d/\tau$, with τ denoting the time constant of the uptake and d the thickness of the molecular container. Approximating these geometric parameters,^[121] the permeability of the photoswitchable top layer was estimated to be $8.5 \times 10^{-11} \text{ m s}^{-1}$ in the *trans* state and $5.4 \times 10^{-12} \text{ m s}^{-1}$ in *cis*. This correlates to an effective diffusion coefficient, which may comprise possible additional transport barriers in the MOF,^[152,154] of $6 \times 10^{-18} \text{ m}^2 \text{ s}^{-1}$ for the *trans* form and $4 \times 10^{-19} \text{ m}^2 \text{ s}^{-1}$ for *cis*. By diffusion switching, this SURMOF hetero-bilayer demonstrated the controlled release from a nanoporous container (Figure 19c).^[121]

Aida and co-workers measured the time-dependent CO_2 uptake in UiO-68 with AB side groups and concluded that the diffusion coefficient in the *trans* state is substantially larger.^[143] For the case of butanediol in $\text{Cu}_2(\text{AzoBPDC})_2(\text{BiPy})$ ^[121] discussed earlier, the switching of the attractive interaction based on the dipole-moment changes of AB, rather than (steric) changes of the pore structure, was identified as the reason for the CO_2 diffusion coefficient changes.

4.3.3. Photoswitching MOF-Based Membrane Permeance and Selectivity

The separation of molecular mixtures by membranes has the potential to tremendously decrease energy consumption and increase efficiency in various fields.^[155] Due to their well-defined nanoporous structure and tunability, MOFs are ideal membrane materials that have been applied successfully in a number of cases.^[155a,156] The performance of a membrane is characterized by the permeance, which describes the flow through the membrane, and the separation factor or selectivity. Generally, the separation of molecular mixtures can be described by the

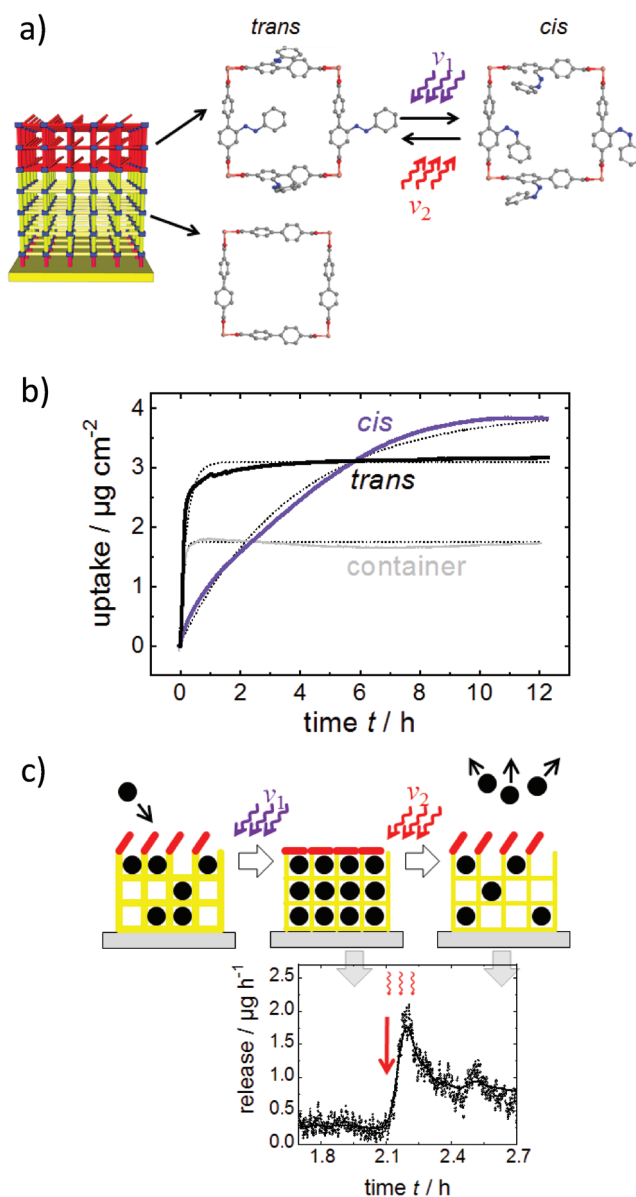


Figure 19. Diffusion switching and remote-controlled release. a) Two-part photoswitchable SURMOF, where the $\text{Cu}_2(\text{BPDC})_2(\text{BiPy})$ bottom layer (yellow) acts as a container for storing molecules, and the photoswitchable $\text{Cu}_2(\text{AzoBPDC})_2(\text{BiPy})$ top layer (red) acts as a valve. Reversible switching occurs from *trans* to *cis* by UV light (ν_1) and from *cis* to *trans* by visible light (ν_2). The sketched pore windows are in the [001] direction. b) Butanediol uptake by the two-layered SURMOF in the *trans* state (black) and in the *cis* state (violet). The time constants of the mono-exponential fits (thin dotted lines) are 0.23 h in the *trans* and 3.6 h in the *cis* state. The uptake by a $\text{Cu}_2(\text{BPDC})_2(\text{BiPy})$ SURMOF is plotted in gray (with a time constant of 0.06 h). c) Release of the guest molecule from the two-layered photoswitchable SURMOF determined by QCM. Beginning at the time indicated by the red arrow, the sample is irradiated with 560 nm wavelength light, initiating the release. a–c) Reproduced with permission.^[121] Copyright 2014, American Chemical Society.

simple relationship membrane selectivity = adsorption selectivity \times diffusion selectivity.^[157] Thus, ideal membrane materials show large differences for the adsorption and/or diffusion of the molecules which should be separated.

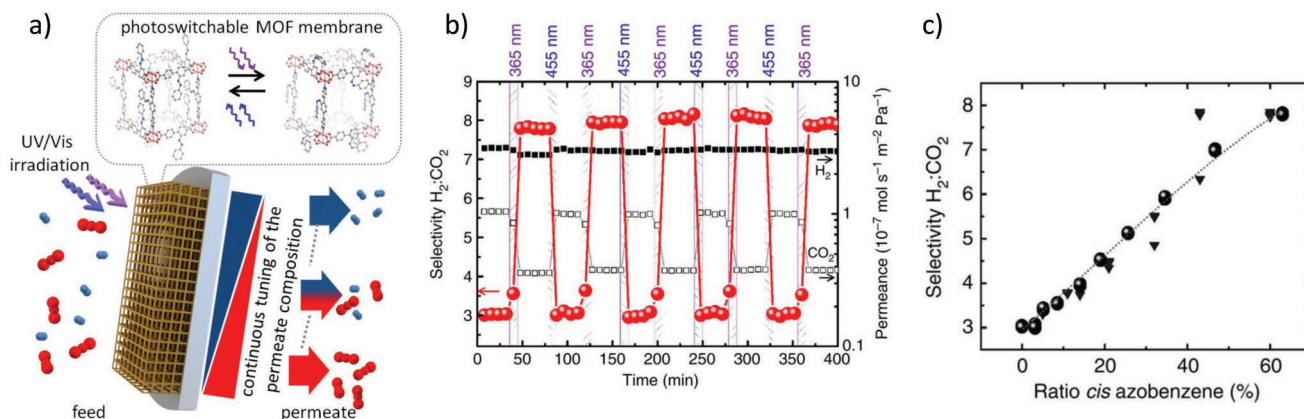


Figure 20. Switchable membrane separation. a) Schematic illustration of tunable, remote-controllable molecular selectivity by a photoswitchable MOF membrane. The molecular feed mixture (red and blue molecules) is separated by the nanoporous membrane. The molecular separation factor, giving the composition of the permeation flux, can be continuously tuned by light irradiation. The structure of $\text{Cu}_2(\text{AzoBPDC})_2(\text{AzoBiPyB})$ with the AB groups *trans* (left) and *cis* (right) is sketched. b) The separation of $\text{H}_2:\text{CO}_2$ mixtures. The membrane is irradiated by 365 and 455 nm light for 5 min each. The permeances of H_2 and CO_2 are shown as black solid squares and black open squares, respectively, with a logarithmic scale on the right-hand side. The molecular selectivities (or separation factors) are shown as red spheres, with the scale on the left-hand side. c) Correlation of the $\text{H}_2:\text{CO}_2$ separation factor with the ratio of *cis* azobenzene. This allows a continuous tuning of the composition of the permeate. a–c) Reproduced under the terms of the CC-BY Creative Commons Attribution 4.0 International License (<http://creativecommons.org/licenses/by/4.0/>).^[104] Copyright 2016, The Authors, published by Springer Nature.

By incorporating photoswitchable moieties in the MOF material, the permeation and separation performance can be modified via remote optical control. The first demonstration of this unique feature of photochromic MOFs was demonstrated for pillared-layer SURMOFs of type $\text{Cu}_2(\text{AzoBPDC})_2(\text{AzoBiPyB})$ with AB side groups. The MOF thin films were grown on mesoporous alumina supports. The molecular membrane separation was determined directly using a Wicke–Kallenbach setup, thus allowing for an operando determination of permeance and selectivity (Figure 20).^[104] The data revealed that, while the H_2 permeance is not influenced by the AB photoisomerization, the CO_2 permeance significantly decreases upon *trans*-to-*cis* switching, reversibly increasing the $\text{H}_2:\text{CO}_2$ separation factor from 3 to 8. In addition to the on-off switching, the AB groups in the membrane can be tuned between the maximum (63%) and minimum (0%) amount of *cis* isomers, for instance, by simultaneous irradiation with blue and UV light. The tuning of the *cis* ratio directly results in a continuous adjustment of the separation factor (Figure 20c).

In a later work, the disadvantage of using UV light was avoided by using SURMOFs of type $\text{Cu}_2(\text{F}_2\text{AzoBDC})_2(\text{dabco})$. In this case, the properties of the photochromic MOF constituents enable modification of the membrane performance and separation factor with visible light.^[117b] This MOF exhibits rather small pores, and thus the steric pore-size effects are expected to dominate the $\text{H}_2:\text{C}_3\text{H}_6$ separation when the selection factor is photomodulated between 9 and 13. On the other hand, the switching of the dipole interaction seems to have a minor influence, and no effect for $\text{H}_2:\text{CO}_2$ was observed, in contrast to the switching performance in a large-pore MOF, $\text{Cu}_2(\text{AzoBPDC})_2(\text{AzoBiPyB})$, where the switching of the attractive (dipole–dipole) interaction causes changes in the separation factor.^[104] Note that the diffusion selectivity seems to dominate the membrane separation in both cases,^[157] whereas the adsorption selectivity has only a minor influence.

In a different approach, Caro and co-workers used the optical switch@MOF approach to apply optical control to membrane performance. They loaded a UiO-67 membrane with AB and demonstrated that simple loading with chromophores is a straightforward alternative for fabricating photoswitchable membranes, avoiding complex organic syntheses of photochromic MOF linkers.^[107b]

In addition to pinhole-free MOF membranes, Katz and co-workers used DAE MOF powder in a filter to separate toluene, naphthalene, and pyrene.^[158]

4.3.4. Photoswitching the Proton Conduction of the Guest Molecules

Proton conductivity of MOFs was intensively investigated, with a focus on sensor and fuel cell applications.^[159] Recently, Müller and co-workers demonstrated that the incorporation of AB moieties in the MOF allows the photomodulation of the proton conductivity in the guest@host matrix.^[117a] For a reproducible proton conductivity measurement, pillared-layer SURMOFs with fluorinated AB side groups were deposited on a substrate already containing an interdigitated electrode, and proton conductivities were measured using impedance spectroscopy. This setup enabled a demonstration of the reversible switching of proton conductivity with visible light, and the influence of different guest molecules, such as butanediol or triazol, on proton transport was investigated. The Nyquist plot and the AC current during the switching (Figure 21c,b) show the reversible modulation of proton conduction properties of the guest molecules as a response to the *trans*–*cis* isomerization of the host MOF. The proton conduction decreases by $\approx 35\%$ upon *trans*-to-*cis* isomerization. This remarkable change is attributed to the stronger attractive interaction of the OH or NH groups with *cis* azobenzene, as shown by infrared spectroscopy and DFT calculations.

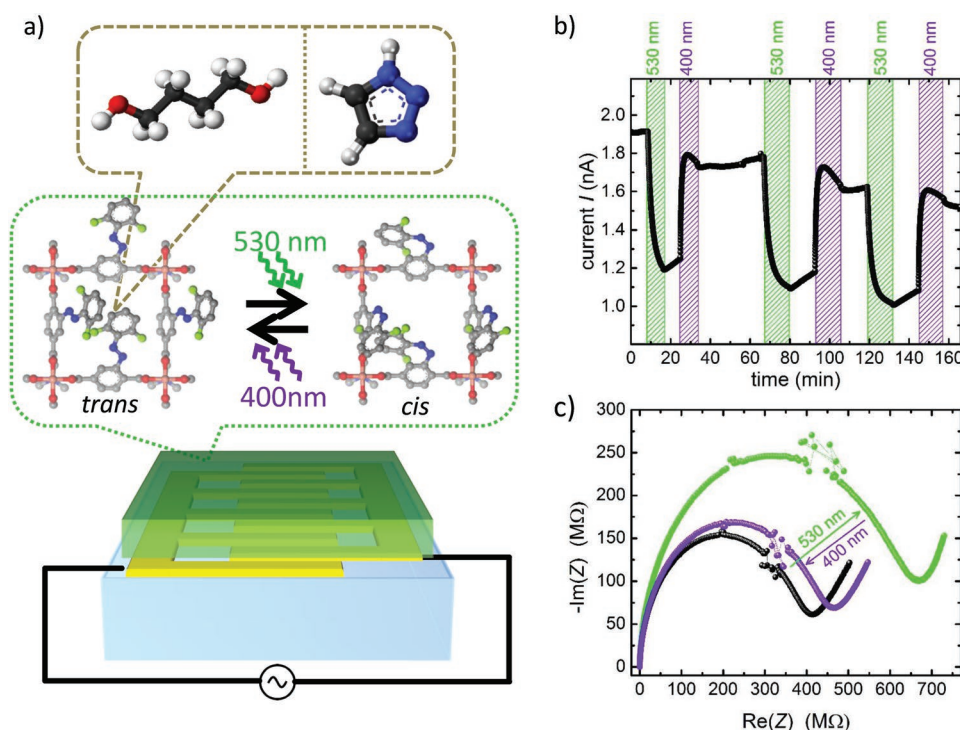


Figure 21. Photoswitchable proton conduction. a) Sketch of the SURMOF film (green) on the interdigitated gold electrodes (yellow) on quartz (light blue) substrate. The $\text{Cu}_2(\text{F}_2\text{AzoBDC})_2(\text{dabco})$ MOF structure with a view along the [001] direction is shown. The fluorinated AB side groups can be switched with green light (530 nm) from *trans* to *cis* and with violet light (400 nm) from *cis* to *trans*. The MOF was filled with 1,4-butanediol or 1,2,3-triazol. The black lines show the connection to the electric circuit and the impedance spectrometer. b) Photoswitchable conduction of butanediol in $\text{Cu}_2(\text{F}_2\text{AzoBDC})_2(\text{dabco})$ SURMOF with the current at a voltage of 1 V and 1 Hz. By irradiation with green light, the AB side groups are switched from the *trans* to the *cis* state. Irradiation with violet light results in a switching to the *trans* state. Three switching cycles of ≈ 9 min (cycle 1) to 12 min (cycles 2 and 3) irradiation time were performed. c) Nyquist plot of impedance Z of butanediol@ $\text{Cu}_2(\text{F}_2\text{AzoBDC})_2(\text{dabco})$. The black data are measured in the pristine sample (*trans*), green after irradiation with green light (*cis*), and violet after irradiation with violet light (*trans*). a–c) Reproduced with permission.^[117a] Copyright 2018, Wiley-VCH.

4.3.5. Photoswitching MOF Catalytic Activity

Due to the large surface area and the possibility of integrating a large density of catalytically active sites, many MOF structures have interesting catalytic properties.^[120,160] The photomodulation of these catalytic properties enables reaction control with high spatial and temporal resolution. For example, the generation of singlet oxygen is of interest for various biological and medical applications, such as photodynamic therapy in cancer treatment.^[161] Feringa and co-workers demonstrated that, in various solutions of DAE and porphyrin, the rate of singlet oxygen generation via a Zn-porphyrin complex can be photomodulated by switching the DAE molecules.^[162] There, the effect is based on the efficient energy transfer from the porphyrin molecule to the closed-ring isomer of DAE, suppressing the formation of singlet oxygen. By pillared-layer MOFs with DAE pillars and Zn-porphyrin linkers, Zhou and co-workers showed that similar excitation transfer correlated with a modification to the singlet oxygen generation can also occur in the crystalline MOF (Figure 22).^[128] They showed that the photoexcitation in the Zn-porphyrin is quickly quenched by transfer to the closed-ring DAE moiety, resulting in a small singlet oxygen generation rate only. When DAE is switched to the open form, this decay channel is effectively blocked, and the singlet

oxygen production rate increases substantially. In a subsequent paper,^[163] the same group demonstrated that this DAE-based MOF can be used to regulate photodynamic therapy, e.g., the destruction of melanoma cells.

5. Conclusion and Outlook

To date, many proof-of-principle studies have demonstrated numerous versatile applications of photoactive MOFs. The fluorescence response of the MOFs and other related photophysical properties including charge transfer, energy transfer, photon upconversion, etc., are intriguing. While in most of the cases the photophysical characterizations were performed with powder form of MOFs, the advantages of thin film structure have also been explored. To realize optoelectronic device applications based on MOF materials, it is fundamentally important to develop suitable material forms that allow a straightforward integration of electrical contacts. At present, thin film fabrication technologies based on layer-by-layer and chemical vapor deposition methods exhibit the largest potential in this context, and should be considered when integrating MOFs into functional devices.

In case of photoswitches, while some of the applications related to the modulation of color and fluorescence^[8,96a,164] have

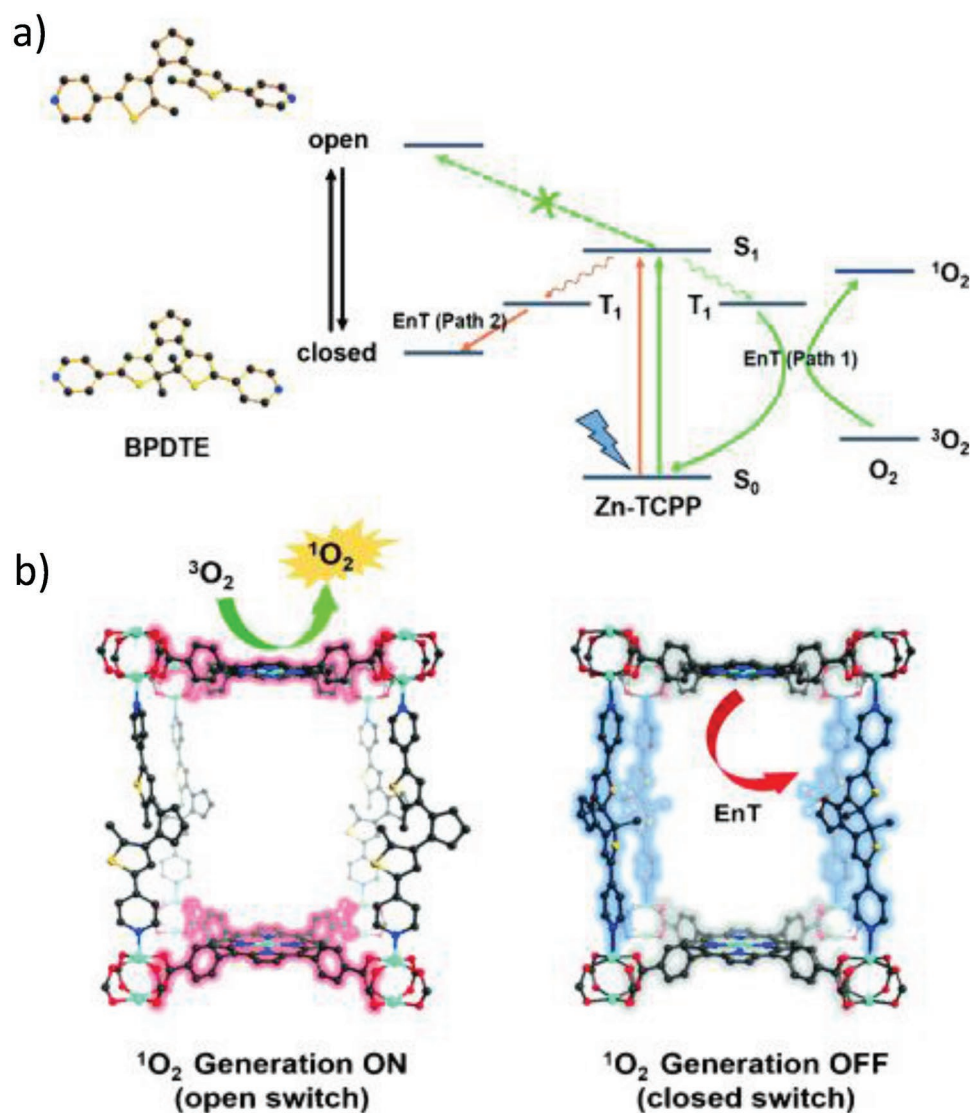


Figure 22. Remote-controllable singlet oxygen production in porphyrin-DAE-MOFs. a) Proposed mechanism of energy transfer (EnT) in SO-PCN. b) Illustration of switching operation in SO-PCN. a,b) Reproduced with permission.^[128] Copyright 2015, Wiley-VCH.

been demonstrated before for other materials, the switching of the adsorption capacity and membrane separation/permeation in MOFs clearly outperforms the switching of these properties in other classes of materials, such as polymers, zeolites, and porous oxides.^[165] Moreover, the remote control of some MOF properties is clearly unprecedented. The photoswitching of proton conduction and the photoswitching of singlet oxygen evolution reaction have not yet been presented before for any solid material. Based on the possibility to integrate virtually any molecule into a MOF, either as a building block or by loading as a guest, we expect further groundbreaking proof-of-principle demonstrations of photoswitching of other properties using MOF materials. In particular, more applications in the fields of information processing and photonics^[166] are anticipated.

In the past, numerous demonstrations of photoswitching in MOFs have used azobenzene as the key component. In the

future, we expect that more frequently other photochromic molecules will be employed, which may be better suited for optimizing existing or establishing new effects. For example, it was demonstrated that the photoswitching of AB results in the creation of a 3 D dipole, which in turn affects the diffusion, membrane separation, and proton conduction. While the size of the AB dipole is already large, other molecules such as spiropyran show changes in dipole moment of more than 10 D. As a result, substantially larger switching effects are expected when integrating these compounds into MOF materials.

We would like to note that in many of previous feasibility studies on photoactive MOF materials, the materials and switching processes were often not sufficiently well characterized. For example, the PSS of photoswitchable MOFs in the form of powder and thin films were quantified only in a few cases, e.g., by NMR,^[143] chromatography,^[122] or by infrared

spectroscopy,^[104,114] while in most studies this important information was not determined. A precise material characterization and a detailed understanding of the MOF material and the switching processes are not only interesting for academic reasons and out of scientific curiosity but also are fundamental for device performance improvements. The lack of reliable information may in part be due to the fact that such information can be difficult to obtain for MOF powders (see Figure 4). In order to avoid these problems, and because of the reasons provided next, we expect that in future applications of MOF-based photoactive materials, thin layers of homogeneous thickness, including SURMOFs, will play a more important role than in the past.

The following points in particular summarize the necessity of the thin film MOFs in order to achieve maximized photoresponse in MOF-based material toward future advanced applications:

- (1) While the molar absorption coefficient of azobenzene is in the range of $10^4 \text{ M}^{-1} \text{ cm}^{-1}$,^[167] the molar absorption coefficient of spiropyran and merocyanine is typically dramatically larger,^[168] resulting in light penetration depths of 1 μm or below. Thus, for particulate forms of MOFs, e.g., in pellets or drop-cast powder suspensions, only the chromophores in the outer surface region of the sintered MOF material can be reached. In contrast, in case of SURMOFs, the thickness can be adjusted to values where essentially all photoactive moieties within the MOF can be excited.
- (2) For electrical contacts required in the context of optoelectronic applications, thin films or SURMOFs deposited on conducting (and at the same time transparent) substrates have substantial advantages over powder forms of MOFs.
- (3) In cases where defect densities play a crucial role, in particular SURMOFs offer a higher quality. In addition, these can be characterized using surface-sensitive techniques like X-ray photoelectron spectroscopy (XPS) in a straightforward fashion.
- (4) The particle size in MOF powders is typically in the micrometer regime, giving rise to strong scattering in the UV and visible regime. Such effects are absent in monolithic MOF thin films, e.g., SURMOFs.
- (5) The fabrication of organic/organic heterointerfaces is important for applications related to, e.g., photon upconversion or charge separation in solar cells. While this is straightforward with layer-by-layer techniques used to fabricate SURMOFs, the realization of well-defined boundaries between different types of MOFs is difficult to achieve with the powder form of MOFs.

Acknowledgements

The authors acknowledge support from Deutsche Forschungsgemeinschaft (DFG, German Research Foundation) under Germany's Excellence Strategy—2082/1—390761711 and SPP 1928 “COORNETS”.

Conflict of Interest

The authors declare no conflict of interest.

Keywords

metal–organic frameworks, photophysics, photoswitching, thin films

Received: August 14, 2019

Revised: October 3, 2019

Published online: November 25, 2019

- [1] a) S. Kitagawa, R. Kitaura, S.-I. Noro, *Angew. Chem., Int. Ed.* **2004**, *43*, 2334; b) H. Furukawa, K. E. Cordova, M. O’Keeffe, O. M. Yaghi, *Science* **2013**, *341*, 1230444.
- [2] S. Grosjean, Z. Hassan, C. Wöll, S. Bräse, *Eur. J. Org. Chem.* **2019**, *2019*, 1446.
- [3] P. Müller, F. M. Wisser, P. Freund, V. Bon, I. Senkovska, S. Kaskel, *Inorg. Chem.* **2017**, *56*, 14164.
- [4] Z.-Z. Lu, R. Zhang, Y.-Z. Li, Z.-J. Guo, H.-G. Zheng, *J. Am. Chem. Soc.* **2011**, *133*, 4172.
- [5] R. Klajn, *Chem. Soc. Rev.* **2014**, *43*, 148.
- [6] A. Bianco, G. Ferrari, R. Castagna, A. Rossi, M. Carminati, G. Pariani, M. Tommasini, C. Bertarelli, *Phys. Chem. Chem. Phys.* **2016**, *18*, 31154.
- [7] A. Marini, A. Muñoz-Losa, A. Biancardi, B. Mennucci, *J. Phys. Chem. B* **2010**, *114*, 17128.
- [8] C. Reichardt, *Chem. Rev.* **1994**, *94*, 2319.
- [9] U. Rösch, S. Yao, R. Wortmann, F. Würthner, *Angew. Chem., Int. Ed.* **2006**, *45*, 7026.
- [10] a) A. Kirchon, L. Feng, H. F. Drake, E. A. Joseph, H.-C. Zhou, *Chem. Soc. Rev.* **2018**, *47*, 8611; b) R. Halder, N. Sikdar, T. K. Maji, *Mater. Today* **2015**, *18*, 97.
- [11] M. P. Suh, H. J. Park, T. K. Prasad, D.-W. Lim, *Chem. Rev.* **2012**, *112*, 782.
- [12] P. Serra-Crespo, T. A. Wezendonk, C. Bach-Samaro, N. Sundar, K. Verouden, M. Zweemer, J. Gascon, H. van den Berg, F. Kapteijn, *Chem. Eng. Technol.* **2015**, *38*, 1183.
- [13] L. Zhu, X.-Q. Liu, H.-L. Jiang, L.-B. Sun, *Chem. Rev.* **2017**, *117*, 8129.
- [14] a) J. Liu, C. Wöll, *Chem. Soc. Rev.* **2017**, *46*, 5730; b) O. Shekhah, H. Wang, S. Kowarik, F. Schreiber, M. Paulus, M. Tolan, C. Sternemann, F. Evers, D. Zacher, R. A. Fischer, C. Wöll, *J. Am. Chem. Soc.* **2007**, *129*, 15118.
- [15] a) L. Heinke, Z. Gu, C. Wöll, *Nat. Commun.* **2014**, *5*, 4562; b) L. Heinke, C. Wöll, *Phys. Chem. Chem. Phys.* **2013**, *15*, 9295.
- [16] E. Virmani, J. M. Rotter, A. Mähringer, T. von Zons, A. Godt, T. Bein, S. Wuttke, D. D. Medina, *J. Am. Chem. Soc.* **2018**, *140*, 4812.
- [17] a) I. Stassen, M. Styles, G. Greci, H. V. Gorp, W. Vanderlinden, S. D. Feyter, P. Falcaro, D. D. Vos, P. Vereecken, R. Ameloot, *Nat. Mater.* **2016**, *15*, 304; b) I. Stassen, D. De Vos, R. Ameloot, *Chem. - Eur. J.* **2016**, *22*, 14452.
- [18] a) B. M. Connolly, M. Aragonés-Anglada, J. Gandara-Loe, N. A. Danaf, D. C. Lamb, J. P. Mehta, D. Vulpe, S. Wuttke, J. Silvestre-Albero, P. Z. Moghadam, A. E. H. Wheatley, D. Fairen-Jimenez, *Nat. Commun.* **2019**, *10*, 2345; b) T. Tian, Z. Zeng, D. Vulpe, M. E. Casco, G. Divitini, P. A. Midgley, J. Silvestre-Albero, J.-C. Tan, P. Z. Moghadam, D. Fairen-Jimenez, *Nat. Mater.* **2018**, *17*, 174; c) T. C. Wang, F. P. Doty, A. I. Benin, J. D. Sugar, W. L. York, E. W. Reinheimer, V. Stavila, M. D. Allendorf, *Chem. Commun.* **2019**, *55*, 4647.
- [19] J.-L. Zhuang, D. Ar, X.-J. Yu, J.-X. Liu, A. Terfort, *Adv. Mater.* **2013**, *25*, 4631.
- [20] A. M. Ullman, C. G. Jones, F. P. Doty, V. Stavila, A. A. Talin, M. D. Allendorf, *ACS Appl. Mater. Interfaces* **2018**, *10*, 24201.
- [21] C. Munuera, O. Shekhah, H. Wang, C. Wöll, C. Ocal, *Phys. Chem. Chem. Phys.* **2008**, *10*, 7257.

- [22] K. Müller, K. Fink, L. Schöttner, M. Koenig, L. Heinke, C. Wöll, *ACS Appl. Mater. Interfaces* **2017**, *9*, 37463.
- [23] Z.-G. Gu, A. Pfriem, S. Hamsch, H. Breitwieser, J. Wohlgemuth, L. Heinke, H. Gliemann, C. Wöll, *Microporous Mesoporous Mater.* **2015**, *211*, 82.
- [24] D. Tanaka, S. Horike, S. Kitagawa, M. Ohba, M. Hasegawa, Y. Ozawa, K. Toriumi, *Chem. Commun.* **2007**, 3142.
- [25] A. Mähringer, A. C. Jakowetz, J. M. Rotter, B. J. Bohn, J. K. Stolarczyk, J. Feldmann, T. Bein, D. D. Medina, *ACS Nano* **2019**, *13*, 6711.
- [26] J. B. Birks, *Nature* **1967**, *214*, 1187.
- [27] C. E. Hoyle, *Photophysics of Polymers*, Vol. 358, American Chemical Society, Washington, DC, USA **1987**, pp. 2–7.
- [28] A. C. Jakowetz, T. F. Hinrichsen, L. Ascherl, T. Sick, M. Calik, F. Auras, D. D. Medina, R. H. Friend, A. Rao, T. Bein, *J. Am. Chem. Soc.* **2019**, *141*, 11565.
- [29] D. Astruc, E. Boisselier, C. Ornelas, *Chem. Rev.* **2010**, *110*, 1857.
- [30] F. Würthner, C. R. Saha-Möller, B. Fimmel, S. Ogi, P. Leowanawat, D. Schmidt, *Chem. Rev.* **2016**, *116*, 962.
- [31] Z. Wang, J. Liu, B. Lukose, Z. Gu, P. G. Weidler, H. Gliemann, T. Heine, C. Wöll, *Nano Lett.* **2014**, *14*, 1526.
- [32] M. C. So, G. P. Wiederrecht, J. E. Mondloch, J. T. Hupp, O. K. Farha, *Chem. Commun.* **2015**, 51, 3501.
- [33] D. E. Williams, N. B. Shustova, *Chem. - Eur. J.* **2015**, *21*, 15474.
- [34] L. E. Kreno, K. Leong, O. K. Farha, M. Allendorf, R. P. Van Duyne, J. T. Hupp, *Chem. Rev.* **2012**, *112*, 1105.
- [35] W. P. Lustig, S. Mukherjee, N. D. Rudd, A. V. Desai, J. Li, S. K. Ghosh, *Chem. Soc. Rev.* **2017**, *46*, 3242.
- [36] I. Stassen, N. Burtch, A. Talin, P. Falcaro, M. Allendorf, R. Ameloot, *Chem. Soc. Rev.* **2017**, *46*, 3185.
- [37] V. Stavila, A. A. Talin, M. D. Allendorf, *Chem. Soc. Rev.* **2014**, *43*, 5994.
- [38] B. L. Chen, Y. Yang, F. Zapata, G. N. Lin, G. D. Qian, E. B. Lobkovsky, *Adv. Mater.* **2007**, *19*, 1693.
- [39] R. Medishetty, J. K. Zareba, D. Mayer, M. Samoc, R. A. Fischer, *Chem. Soc. Rev.* **2017**, *46*, 4976.
- [40] Y. J. Cui, Y. F. Yue, G. D. Qian, B. L. Chen, *Chem. Rev.* **2012**, *112*, 1126.
- [41] M. D. Allendorf, C. A. Bauer, R. K. Bhakta, R. J. T. Houk, *Chem. Soc. Rev.* **2009**, *38*, 1330.
- [42] W. P. Lustig, J. Li, *Coord. Chem. Rev.* **2018**, *373*, 116.
- [43] C. A. Bauer, T. V. Timofeeva, T. B. Settersten, B. D. Patterson, V. H. Liu, B. A. Simmons, M. D. Allendorf, *J. Am. Chem. Soc.* **2007**, *129*, 7136.
- [44] K. C. Stylianou, R. Heck, S. Y. Chong, J. Bacsá, J. T. A. Jones, Y. Z. Khimyak, D. Bradshaw, M. J. Rosseinsky, *J. Am. Chem. Soc.* **2010**, *132*, 4119.
- [45] N. B. Shustova, B. D. McCarthy, M. Dincă, *J. Am. Chem. Soc.* **2011**, *133*, 20126.
- [46] N. B. Shustova, A. F. Cozzolino, M. Dincă, *J. Am. Chem. Soc.* **2012**, *134*, 19596.
- [47] N. B. Shustova, T.-C. Ong, A. F. Cozzolino, V. K. Michaelis, R. G. Griffin, M. Dincă, *J. Am. Chem. Soc.* **2012**, *134*, 15061.
- [48] Z. Wei, Z.-Y. Gu, R. K. Arvapally, Y.-P. Chen, R. N. McDougald, J. F. Ivy, A. A. Yakovenko, D. Feng, M. A. Omary, H.-C. Zhou, *J. Am. Chem. Soc.* **2014**, *136*, 8269.
- [49] U. Mitschke, P. Bäuerle, *J. Mater. Chem.* **2000**, *10*, 1471.
- [50] H. Uoyama, K. Goushi, K. Shizu, H. Nomura, C. Adachi, *Nature* **2012**, *492*, 234.
- [51] Z. Hu, G. Huang, W. P. Lustig, F. Wang, H. Wang, S. J. Teat, D. Banerjee, D. Zhang, J. Li, *Chem. Commun.* **2015**, 51, 3045.
- [52] R. Haldar, S. Diring, P. K. Samanta, M. Muth, W. Clancy, A. Mazel, S. Schlabach, F. Kirschhöfer, G. Brenner-Weiß, S. K. Pati, F. Odobel, C. Wöll, *Angew. Chem., Int. Ed.* **2018**, *57*, 13662.
- [53] a) R. Haldar, A. Mazel, R. Joseph, M. Adams, I. A. Howard, B. S. Richards, M. Tsotsalas, E. Redel, S. Diring, F. Odobel, C. Wöll, *Chem. - Eur. J.* **2017**, *23*, 14316; b) R. Haldar, A. Mazel, M. Krstić, Q. Zhang, M. Jakoby, I. A. Howard, B. S. Richards, N. Jung, D. Jacquemin, S. Diring, W. Wenzel, F. Odobel, C. Wöll, *Nat. Commun.* **2019**, *10*, 2048.
- [54] N. Sikdar, D. Dutta, R. Haldar, T. Ray, A. Hazra, A. J. Bhattacharyya, T. K. Maji, *J. Phys. Chem. C* **2016**, *120*, 13622.
- [55] B. Rühle, E. Virmani, H. Engelke, F. M. Hinterholzinger, T. von Zons, B. Brosent, T. Bein, A. Godt, S. Wuttke, *Chem. - Eur. J.* **2019**, *25*, 6349.
- [56] Z. Jin, G. S. Zhu, Y. C. Zou, Q. R. Fang, M. Xue, Z. Y. Li, S. L. Qiu, *J. Mol. Struct.* **2007**, *871*, 80.
- [57] X.-H. Chang, Y. Zhao, X. Feng, L.-F. Ma, L.-Y. Wang, *Polyhedron* **2014**, *83*, 159.
- [58] C. Y. Gao, D. Wang, J. P. Li, Y. Wang, W. T. Yang, *CrystEngComm* **2016**, *18*, 2857.
- [59] A. Salehi, X. Fu, D.-H. Shin, F. So, *Adv. Funct. Mater.* **2019**, *29*, 1808803.
- [60] Y. J. Cui, B. L. Chen, G. D. Qian, *Coord. Chem. Rev.* **2014**, *273*, 76.
- [61] S. Yuan, Y.-K. Deng, D. Sun, *Chem. - Eur. J.* **2014**, *20*, 10093.
- [62] X. Yang, D. Yan, *Chem. Sci.* **2016**, *7*, 4519.
- [63] H. Mieno, R. Kabe, N. Notsuka, M. D. Allendorf, C. Adachi, *Adv. Opt. Mater.* **2016**, *4*, 1015.
- [64] H. Mieno, R. Kabe, M. D. Allendorf, C. Adachi, *Chem. Commun.* **2018**, *54*, 631.
- [65] N. Baroni, A. Turshatov, M. Adams, E. A. Dolgoplova, S. Schliske, G. Hernandez-Sosa, C. Wöll, N. B. Shustova, B. S. Richards, I. A. Howard, *ACS Appl. Mater. Interfaces* **2018**, *10*, 25754.
- [66] M. Gutiérrez, F. Sánchez, A. Douhal, *Phys. Chem. Chem. Phys.* **2016**, *18*, 5112.
- [67] S. A. Odom, M. M. Caruso, A. D. Finke, A. M. Prokup, J. A. Ritchey, J. H. Leonard, S. R. White, N. R. Sottos, J. S. Moore, *Adv. Funct. Mater.* **2010**, *20*, 1721.
- [68] P. L. Feng, K. Leong, M. D. Allendorf, *Dalton Trans.* **2012**, *41*, 8869.
- [69] a) G. J. McManus, Perry, M. Perry, B. D. Wagner, M. J. Zaworotko, *J. Am. Chem. Soc.* **2007**, *129*, 9094; b) B. D. Wagner, G. J. McManus, B. Moulton, M. J. Zaworotko, *Chem. Commun.* **2002**, 2176.
- [70] Y. Takashima, V. M. Martínez, S. Furukawa, M. Kondo, S. Shimomura, H. Uehara, M. Nakahama, K. Sugimoto, S. Kitagawa, *Nat. Commun.* **2011**, *2*, 168.
- [71] V. Martínez-Martínez, S. Furukawa, Y. Takashima, I. López Arbeloa, S. Kitagawa, *J. Phys. Chem. C* **2012**, *116*, 26084.
- [72] R. Haldar, R. Matsuda, S. Kitagawa, S. J. George, T. K. Maji, *Angew. Chem., Int. Ed.* **2014**, *53*, 11772.
- [73] T. Tsukamoto, K. Takada, R. Sakamoto, R. Matsuoka, R. Toyoda, H. Maeda, T. Yagi, M. Nishikawa, N. Shinjo, S. Amano, T. Iokawa, N. Ishibashi, T. Oi, K. Kanayama, R. Kinugawa, Y. Koda, T. Komura, S. Nakajima, R. Fukuyama, N. Fuse, M. Mizui, M. Miyasaki, Y. Yamashita, K. Yamada, W. Zhang, R. Han, W. Liu, T. Tsubomura, H. Nishihara, *J. Am. Chem. Soc.* **2017**, *139*, 5359.
- [74] E. Castaldelli, K. D. G. I. Jayawardena, D. C. Cox, G. J. Clarkson, R. I. Walton, L. Le-Quang, J. Chauvin, S. R. P. Silva, G. J.-F. Demets, *Nat. Commun.* **2017**, *8*, 2139.
- [75] X. Liu, M. Kozłowska, T. Okkali, D. Wagner, T. Higashino, G. Brenner-Weiß, S. M. Marschner, Z. Fu, Q. Zhang, H. Imahori, S. Bräse, W. Wenzel, C. Wöll, L. Heinke, *Angew. Chem., Int. Ed.* **2019**, *58*, 9590.
- [76] a) J. Liu, W. Zhou, J. Liu, I. Howard, G. Kilbarda, S. Schlabach, D. Coupy, M. Addicoat, S. Yoneda, Y. Tsutsui, T. Sakurai, S. Seki, Z. Wang, P. Lindemann, E. Redel, T. Heine, C. Wöll, *Angew. Chem., Int. Ed.* **2015**, *54*, 7441; b) J. Liu, W. Zhou, J. Liu, Y. Fujimori, T. Higashino, H. Imahori, X. Jiang, J. Zhao, T. Sakurai, Y. Hattori,

- W. Matsuda, S. Seki, S. K. Garlapati, S. Dasgupta, E. Redel, L. Sun, C. Wöll, *J. Mater. Chem. A* **2016**, *4*, 12739.
- [77] R. Haldar, K. Batra, S. M. Marschner, A. B. Kuc, S. Zahn, R. A. Fischer, S. Bräse, T. Heine, C. Wöll, *Chem. - Eur. J.* **2019**, *25*, 7847.
- [78] R. Sakamoto, K. Hoshiko, Q. Liu, T. Yagi, T. Nagayama, S. Kusaka, M. Tsuchiya, Y. Kitagawa, W.-Y. Wong, H. Nishihara, *Nat. Commun.* **2015**, *6*, 6713.
- [79] N. Sikdar, K. Jayaramulu, V. Kiran, K. V. Rao, S. Sampath, S. J. George, T. K. Maji, *Chem. - Eur. J.* **2015**, *21*, 11701.
- [80] C. Y. Lee, O. K. Farha, B. J. Hong, A. A. Sarjeant, S. T. Nguyen, J. T. Hupp, *J. Am. Chem. Soc.* **2011**, *133*, 15858.
- [81] H.-J. Son, S. Jin, S. Patwardhan, S. J. Wezenberg, N. C. Jeong, M. So, C. E. Wilmer, A. A. Sarjeant, G. C. Schatz, R. Q. Snurr, O. K. Farha, G. P. Wiederrecht, J. T. Hupp, *J. Am. Chem. Soc.* **2013**, *135*, 862.
- [82] Q. Q. Zhang, C. K. Zhang, L. Y. Cao, Z. Wang, B. An, Z. K. Lin, R. Y. Huang, Z. M. Zhang, C. Wang, W. B. Lin, *J. Am. Chem. Soc.* **2016**, *138*, 5308.
- [83] J. Liu, B. Lukose, O. Shekhah, H. K. Arslan, P. Weidler, H. Gliemann, S. Bräse, S. Grosjean, A. Godt, X. Feng, K. Müllen, I.-B. Magdau, T. Heine, C. Wöll, *Sci. Rep.* **2012**, *2*, 921.
- [84] R. Haldar, M. Jakoby, A. Mazel, Q. Zhang, A. Welle, T. Mohamed, P. Krolla, W. Wenzel, S. Diring, F. Odobel, B. S. Richards, I. A. Howard, C. Wöll, *Nat. Commun.* **2018**, *9*, 4332.
- [85] E. A. Dolgoplova, D. E. Williams, A. B. Greytak, A. M. Rice, M. D. Smith, J. A. Krause, N. B. Shustova, *Angew. Chem., Int. Ed.* **2015**, *54*, 13639.
- [86] S. Y. Jin, H. J. Son, O. K. Farha, G. P. Wiederrecht, J. T. Hupp, *J. Am. Chem. Soc.* **2013**, *135*, 955.
- [87] H. J. Park, M. C. So, D. Gosztola, G. P. Wiederrecht, J. D. Emery, A. B. F. Martinson, S. Er, C. E. Wilmer, N. A. Vermeulen, A. Aspuru-Guzik, J. F. Stoddart, O. K. Farha, J. T. Hupp, *ACS Appl. Mater. Interfaces* **2016**, *8*, 24983.
- [88] S. Goswami, L. Ma, A. B. F. Martinson, M. R. Wasielewski, O. K. Farha, J. T. Hupp, *ACS Appl. Mater. Interfaces* **2016**, *8*, 30863.
- [89] a) X.-L. Hu, C. Qin, X.-L. Wang, K.-Z. Shao, Z.-M. Su, *Chem. Commun.* **2015**, *51*, 17521; b) Y. Cui, R. Song, J. Yu, M. Liu, Z. Wang, C. Wu, Y. Yang, Z. Wang, B. Chen, G. Qian, *Adv. Mater.* **2015**, *27*, 1420; c) R. Haldar, K. Prasad, A. Hazra, T. K. Maji, *Cryst. Growth Des.* **2019**, *19*, 1514; d) K. Leong, M. E. Foster, B. M. Wong, E. D. Spoeke, D. Van Gough, J. C. Deaton, M. D. Allendorf, *J. Mater. Chem. A* **2014**, *2*, 3389.
- [90] a) M. Oldenburg, A. Turshatov, D. Busko, S. Wollgarten, M. Adams, N. Baroni, A. Welle, E. Redel, C. Wöll, B. S. Richards, I. A. Howard, *Adv. Mater.* **2016**, *28*, 8477; b) S. Ahmad, J. Liu, C. Gong, J. Zhao, L. Sun, *ACS Appl. Energy Mater.* **2018**, *1*, 249.
- [91] P. Mahato, A. Monguzzi, N. Yanai, T. Yamada, N. Kimizuka, *Nat. Mater.* **2015**, *14*, 924.
- [92] P. Mahato, A. Monguzzi, N. Yanai, T. Yamada, N. Kimizuka, *Nat. Mater.* **2017**, *16*, 153.
- [93] M. Adams, M. Kozłowska, N. Baroni, M. Oldenburg, R. Ma, D. Busko, A. Turshatov, G. Emandi, M. O. Senge, R. Haldar, C. Woll, G. U. Nienhaus, B. S. Richards, I. A. Howard, *ACS Appl. Mater. Interfaces* **2019**, *11*, 15688.
- [94] a) L. Poisson, K. D. Raffael, B. Soep, J. M. Mestdagh, G. Buntinx, *J. Am. Chem. Soc.* **2006**, *128*, 3169; b) E. M. M. Tan, S. Amirjalayer, S. Smolarek, A. Vdovin, F. Zerbetto, W. J. Buma, *Nat. Commun.* **2015**, *6*, 7; c) M. S. Scholz, J. N. Bull, N. J. A. Coughlan, E. Carrascosa, B. D. Adamson, E. J. Bieske, *J. Phys. Chem. A* **2017**, *121*, 6413.
- [95] a) M. Gobbi, S. Bonacchi, J. X. Lian, A. Vercouter, S. Bertolazzi, B. Zyska, M. Timpel, R. Tatti, Y. Olivier, S. Hecht, M. V. Nardi, D. Beljonne, E. Orgiu, P. Samorì, *Nat. Commun.* **2018**, *9*, 2661; b) Y. Zhao, S. Bertolazzi, P. Samorì, *ACS Nano* **2019**, *13*, 4814.
- [96] a) H. M. D. Bandara, S. C. Burdette, *Chem. Soc. Rev.* **2012**, *41*, 1809; b) F. D. Jochum, P. Theato, *Chem. Soc. Rev.* **2013**, *42*, 7468; c) T. Ikeda, J. Mamiya, Y. L. Yu, *Angew. Chem., Int. Ed.* **2007**, *46*, 506.
- [97] A. Modrow, D. Zargarani, R. Herges, N. Stock, *Dalton Trans.* **2011**, *40*, 4217.
- [98] a) A. Modrow, D. Zargarani, R. Herges, N. Stock, *Dalton Trans.* **2012**, *41*, 8690; b) J. Park, D. Q. Yuan, K. T. Pham, J. R. Li, A. Yakovenko, H. C. Zhou, *J. Am. Chem. Soc.* **2012**, *134*, 99.
- [99] X. Lin, T. Liu, J. Lin, H. Yang, J. Lue, B. Xu, R. Cao, *Inorg. Chem. Commun.* **2010**, *13*, 388.
- [100] W. Danowski, T. van Leeuwen, S. Abdolazadeh, D. Roke, W. R. Browne, S. Wezenberg, B. L. Feringa, *Nat. Nanotechnol.* **2019**, *14*, 488.
- [101] a) G. Mehlana, S. A. Bourne, *CrystEngComm* **2017**, *19*, 4238; b) C. L. Jones, A. J. Tansell, T. L. Easun, *J. Mater. Chem. A* **2016**, *4*, 6714; c) S. Castellanos, F. Kapteijn, J. Gascon, *CrystEngComm* **2016**, *18*, 4006; d) O. S. Bushuyev, T. Friscic, C. J. Barrett, *CrystEngComm* **2016**, *18*, 7204; e) A. Knebel, C. Zhou, A. S. Huang, J. Zhang, L. Kustov, J. Caro, *Chem. Eng. Technol.* **2018**, *41*, 224; f) R. D. Mukhopadhyay, V. K. Praveen, A. Ajayaghosh, *Mater. Horiz.* **2014**, *1*, 572; g) A. B. Kanj, K. Müller, L. Heinke, *Macromol. Rapid Commun.* **2017**, *38*, 1700239; h) H. A. Schwartz, U. Ruschewitz, L. Heinke, *Photochem. Photobiol. Sci.* **2018**, *17*, 864.
- [102] D. Hermann, H. Emerich, R. Lepski, D. Schaniel, U. Ruschewitz, *Inorg. Chem.* **2013**, *52*, 2744.
- [103] C. C. Epley, K. L. Roth, S. Y. Lin, S. R. Ahrenholtz, T. Z. Grove, A. J. Morris, *Dalton Trans.* **2017**, *46*, 4917.
- [104] Z. Wang, A. Knebel, S. Grosjean, D. Wagner, S. Bräse, C. Wöll, J. Caro, L. Heinke, *Nat. Commun.* **2016**, *7*, 13872.
- [105] K. Müller, J. Wadhwa, J. S. Malhi, L. Schöttner, A. Welle, H. Schwartz, D. Hermann, U. Ruschewitz, L. Heinke, *Chem. Commun.* **2017**, *53*, 8070.
- [106] H. A. Schwartz, S. Olthof, D. Schaniel, K. Meerholz, U. Ruschewitz, *Inorg. Chem.* **2017**, *56*, 13100.
- [107] a) N. Yanai, T. Uemura, M. Inoue, R. Matsuda, T. Fukushima, M. Tsujimoto, S. Isoda, S. Kitagawa, *J. Am. Chem. Soc.* **2012**, *134*, 4501; b) A. Knebel, L. Sundermann, A. Mohmeyer, I. Strauss, S. Friebe, P. Behrens, J. Caro, *Chem. Mater.* **2017**, *29*, 3111.
- [108] a) V. V. Semionova, V. V. Korolev, E. M. Glebov, V. Z. Shirinyan, S. A. Sapchenko, *J. Struct. Chem.* **2016**, *57*, 1216; b) I. M. Walton, J. M. Cox, J. A. Coppin, C. M. Linderman, D. G. Patel, J. B. Benedict, *Chem. Commun.* **2013**, *49*, 8012.
- [109] a) S. Garg, H. Schwartz, M. Kozłowska, A. B. Kanj, K. Müller, W. Wenzel, U. Ruschewitz, L. Heinke, *Angew. Chem., Int. Ed.* **2019**, *58*, 1193; b) U. G. R. Lakmali, C. V. Hettiarachchi, *CrystEngComm* **2015**, *17*, 8607; c) F. Zhang, X. Q. Zou, W. Feng, X. J. Zhao, X. F. Jing, F. X. Sun, H. Ren, G. S. Zhu, *J. Mater. Chem.* **2012**, *22*, 25019.
- [110] H. Agarkar, D. Das, *J. Mol. Struct.* **2019**, *1184*, 435.
- [111] K. Healey, W. B. Liang, P. D. Southon, T. L. Church, D. M. D'Alessandro, *J. Mater. Chem. A* **2016**, *4*, 10816.
- [112] Z. Wang, L. Heinke, J. Jelic, M. Cakici, M. Dommaschk, R. J. Maurer, H. Oberhofer, S. Grosjean, R. Herges, S. Bräse, K. Reuter, C. Wöll, *Phys. Chem. Chem. Phys.* **2015**, *17*, 14582.
- [113] S. Castellanos, A. Goulet-Hanssens, F. Zhao, A. Dikhtiarenko, A. Pustovarenko, S. Hecht, J. Gascon, F. Kapteijn, D. Blegler, *Chem. - Eur. J.* **2016**, *22*, 746.
- [114] X. Yu, Z. Wang, M. Buchholz, N. Fullgrabe, S. Grosjean, F. Bebensee, S. Bräse, C. Wöll, L. Heinke, *Phys. Chem. Chem. Phys.* **2015**, *17*, 22721.
- [115] W. Zhou, S. Grosjean, S. Bräse, L. Heinke, *Z. Phys. Chem.* **2019**, *233*, 15.
- [116] D. Blegler, J. Schwarz, A. M. Brouwer, S. Hecht, *J. Am. Chem. Soc.* **2012**, *134*, 20597.

- [117] a) K. Müller, J. Helfferich, F. L. Zhao, R. Verma, A. B. Kanj, V. Meded, D. Bléger, W. Wenzel, L. Heinke, *Adv. Mater.* **2018**, *30*, 1706551; b) K. Müller, A. Knebel, F. Zhao, D. Bléger, J. Caro, L. Heinke, *Chem. - Eur. J.* **2017**, *23*, 5434.
- [118] a) I. M. Walton, J. M. Cox, C. A. Benson, D. G. Patel, Y.-S. Chen, J. B. Benedict, *New J. Chem.* **2016**, *40*, 101; b) D. G. Patel, I. M. Walton, J. M. Cox, C. J. Gleason, D. R. Butzer, J. B. Benedict, *Chem. Commun.* **2014**, *50*, 2653.
- [119] E. A. Dolgoplova, V. A. Galitskiy, C. R. Martin, H. N. Gregory, B. J. Yarbrough, A. M. Rice, A. A. Berseneva, O. A. Elegbavwo, K. S. Stephenson, P. Kittikhunnatham, S. G. Karakalos, M. D. Smith, A. B. Greytak, S. Garashchuk, N. B. Shustova, *J. Am. Chem. Soc.* **2019**, *141*, 5350.
- [120] Z. Wang, C. Woell, *Adv. Mater. Technol.* **2019**, *4*.
- [121] L. Heinke, M. Cakici, M. Dommaschk, S. Grosjean, R. Herges, S. Bräse, C. Wöll, *ACS Nano* **2014**, *8*, 1463.
- [122] D. Mutruc, A. Goulet-Hanssens, S. Fairman, S. Wahl, A. Zimathies, C. Knie, S. Hecht, *Angew. Chem., Int. Ed.* **2019**, *58*, 12862.
- [123] X. Meng, B. Gui, D. Yuan, M. Zeller, C. Wang, *Sci. Adv.* **2016**, *2*, e1600480.
- [124] M. Irie, T. Fulcaminato, K. Matsuda, S. Kobatake, *Chem. Rev.* **2014**, *114*, 12174.
- [125] V. I. Nikolayenko, S. A. Herbert, L. J. Barbour, *Chem. Commun.* **2017**, *53*, 11142.
- [126] Y. Zheng, H. Sato, P. Wu, H. J. Jeon, R. Matsuda, S. Kitagawa, *Nat. Commun.* **2017**, *8*, 100.
- [127] C. B. Fan, L. L. Gong, L. Huang, F. Luo, R. Krishna, X. F. Yi, A. M. Zheng, L. Zhang, S. Z. Pu, X. F. Feng, M. B. Luo, G. C. Guo, *Angew. Chem., Int. Ed.* **2017**, *56*, 7900.
- [128] J. Park, D. Feng, S. Yuan, H.-C. Zhou, *Angew. Chem., Int. Ed.* **2015**, *54*, 430.
- [129] A. Schaate, S. Duhnen, G. Platz, S. Lilienthal, A. M. Schneider, P. Behrens, *Eur. J. Inorg. Chem.* **2012**, *2012*, 790.
- [130] a) J. Zhang, L. Wang, N. Li, J. Liu, W. Zhang, Z. Zhang, N. Zhou, X. Zhu, *CrystEngComm* **2014**, *16*, 6547; b) C. Liu, W. Zhang, Q. Zeng, S. Lei, *Chem. - Eur. J.* **2016**, *22*, 6768.
- [131] R. D. Mukhopadhyay, V. K. Praveen, A. Hazra, T. K. Maji, A. Ajayaghosh, *Chem. Sci.* **2015**, *6*, 6583.
- [132] a) R. Lyndon, K. Konstas, B. P. Ladewig, P. D. Southon, P. C. J. Kepert, M. R. Hill, *Angew. Chem., Int. Ed.* **2013**, *52*, 3695; b) L. L. Gong, X. F. Feng, F. Luo, *Inorg. Chem.* **2015**, *54*, 11587; c) H. Li, M. R. Martinez, Z. Perry, H.-C. Zhou, P. Falcaro, C. Doblin, S. Lim, A. J. Hill, B. Halstead, M. R. Hill, *Chem. - Eur. J.* **2016**, *22*, 11176.
- [133] D. E. Williams, C. R. Martin, E. A. Dolgoplova, A. Swifton, D. C. Godfrey, O. A. Ejegbavwo, P. J. Pellechia, M. D. Smith, N. B. Shustova, *J. Am. Chem. Soc.* **2018**, *140*, 7611.
- [134] P. K. Kundu, G. L. Olsen, V. Kiss, R. Klajn, *Nat. Commun.* **2014**, *5*, 3588.
- [135] I. Stassen, N. C. Burtch, A. A. Talin, P. Falcaro, M. D. Allendorf, R. Ameloot, *Chem. Soc. Rev.* **2017**, *46*, 3853.
- [136] a) N. Darwish, A. C. Aragonés, T. Darwish, S. Ciampi, I. Diez-Perez, *Nano Lett.* **2014**, *14*, 7064; b) S. Kumar, J. T. van Herp, R. Y. N. Gengler, B. L. Feringa, P. Rudolf, R. C. Chiechi, *J. Am. Chem. Soc.* **2016**, *138*, 12519.
- [137] R. A. Marcus, *Rev. Mod. Phys.* **1993**, *65*, 599.
- [138] E. Coronado, G. M. Espallargas, *Chem. Soc. Rev.* **2013**, *42*, 1525.
- [139] G. Minguez Espallargas, E. Coronado, *Chem. Soc. Rev.* **2018**, *47*, 533.
- [140] H. Meng, C. Zhao, M. Nie, C. Wang, T. Wang, *ACS Appl. Mater. Interfaces* **2018**, *10*, 32607.
- [141] Z. Wang, S. Grosjean, S. Bräse, L. Heinke, *ChemPhysChem* **2015**, *16*, 3779.
- [142] a) Z. B. Wang, K. Müller, M. Valasek, S. Grosjean, S. Bräse, C. Wöll, M. Mayor, L. Heinke, *J. Phys. Chem. C* **2018**, *122*, 19044; b) Y. Zhu, W. Zhang, *Chem. Sci.* **2014**, *5*, 4957.
- [143] H. B. Huang, H. Sato, T. Aida, *J. Am. Chem. Soc.* **2017**, *139*, 8784.
- [144] R. Yuan, H. Ren, H. He, L. Jiang, G. Zhu, *Sci. China Mater.* **2015**, *58*, 38.
- [145] C. T. Yang, A. R. Kshirsagar, A. C. Eddin, L. C. Lin, R. Poloni, *Chem. - Eur. J.* **2018**, *24*, 15167.
- [146] J. S. Caddy, T. B. Faust, I. M. Walton, J. M. Cox, J. B. Benedict, M. B. Solomon, P. D. Southon, C. J. Kepert, D. M. D'Alessandro, *Aust. J. Chem.* **2017**, *70*, 1171.
- [147] a) C. B. Fan, Z. Q. Liu, L. L. Gong, A. M. Zheng, L. Zhang, C. S. Yan, H. Q. Wu, X. F. Feng, F. Luo, *Chem. Commun.* **2017**, *53*, 763; b) R. Lyndon, K. Konstas, R. A. Evans, D. J. Keddie, M. R. Hill, B. P. Ladewig, *Adv. Funct. Mater.* **2015**, *25*, 4405; c) F. Luo, C. B. Fan, M. B. Luo, X. L. Wu, Y. Zhu, S. Z. Pu, W.-Y. Xu, G.-C. Guo, *Angew. Chem., Int. Ed.* **2014**, *53*, 9298.
- [148] Y. Jiang, P. Tan, S.-C. Qi, X.-Q. Liu, J.-H. Yan, F. Fan, L.-B. Sun, *Angew. Chem., Int. Ed.* **2019**, *58*, 6600.
- [149] L. Cheng, Y. Jiang, S.-C. Qi, W. Liu, S.-F. Shan, P. Tan, X.-Q. Liu, L.-B. Sun, *Chem. Mater.* **2018**, *30*, 3429.
- [150] A. B. Kanj, J. Bürck, S. Grosjean, S. Bräse, L. Heinke, *Chem. Commun.* **2019**, *55*, 8776.
- [151] J. Brown, B. L. Henderson, M. D. Kiesz, A. C. Whalley, W. Morris, S. Grunder, H. Deng, H. Furukawa, J. I. Zink, J. F. Stoddart, O. M. Yaghi, *Chem. Sci.* **2013**, *4*, 2858.
- [152] J. Kärger, D. M. Ruthven, D. N. Theodorou, *Diffusion in Nanoporous Materials*, Wiley-VCH, Weinheim, Germany **2012**.
- [153] a) D. Johannsmann, *The Quartz Crystal Microbalance in Soft Matter Research*, Springer, Berlin, Germany **2015**; b) L. Heinke, *J. Phys. D: Appl. Phys.* **2017**, *50*, 193004.
- [154] F. Hibbe, C. Chmelik, L. Heinke, S. Pramanik, J. Li, D. M. Ruthven, D. Tzoulaki, J. Kärger, *J. Am. Chem. Soc.* **2011**, *133*, 2804.
- [155] a) N. Rangnekar, N. Mittal, B. Elyassi, J. Caro, M. Tsapatsis, *Chem. Soc. Rev.* **2015**, *44*, 7128; b) J. Caro, M. Noack, *Microporous Mesoporous Mater.* **2008**, *115*, 215.
- [156] a) S. Qiu, M. Xue, G. Zhu, *Chem. Soc. Rev.* **2014**, *43*, 6116; b) S. Hurrell, S. Friebe, J. Wohlgemuth, C. Wöll, J. Caro, L. Heinke, *Chem. - Eur. J.* **2017**, *23*, 2294; c) T. Rodenas, I. Luz, G. Prieto, B. Seoane, H. Miro, A. Corma, F. Kapteijn, F. X. Llabrés i Xamena, J. Gascon, *Nat. Mater.* **2015**, *14*, 48.
- [157] C. Chmelik, H. Bux, H. Voss, J. Caro, *Chem. Ing. Tech.* **2011**, *83*, 104.
- [158] B. J. Furlong, M. J. Katz, *J. Am. Chem. Soc.* **2017**, *139*, 13280.
- [159] a) M. Yoon, K. Suh, S. Natarajan, K. Kim, *Angew. Chem., Int. Ed.* **2013**, *52*, 2688; b) J. M. Taylor, R. K. Mah, I. L. Moudrakovski, C. I. Ratcliffe, R. Vaidhyanathan, G. K. H. Shimizu, *J. Am. Chem. Soc.* **2010**, *132*, 14055; c) J. A. Hurd, R. Vaidhyanathan, V. Thangadurai, C. I. Ratcliffe, I. L. Moudrakovski, G. K. H. Shimizu, *Nat. Chem.* **2009**, *1*, 705.
- [160] A. Dhakshinamoorthy, Z. H. Li, H. Garcia, *Chem. Soc. Rev.* **2018**, *47*, 8134.
- [161] M. C. DeRosa, R. J. Crutchley, *Coord. Chem. Rev.* **2002**, *233-234*, 351.
- [162] L. Hou, X. Zhang, T. C. Pijper, W. R. Browne, B. L. Feringa, *J. Am. Chem. Soc.* **2014**, *136*, 910.
- [163] J. Park, Q. Jiang, D. Feng, H.-C. Zhou, *Angew. Chem., Int. Ed.* **2016**, *55*, 7188.
- [164] M.-M. Russew, S. Hecht, *Adv. Mater.* **2010**, *22*, 3348.
- [165] a) M. Alvaro, M. Benitez, D. Das, H. Garcia, E. Peris, *Chem. Mater.* **2005**, *17*, 4958; b) K. Weh, M. Noack, K. Hoffmann, K. P. Schröder, J. Caro, *Microporous Mesoporous Mater.* **2002**, *54*, 15.
- [166] Z. Zhang, K. Müller, S. Heidrich, M. Koenig, T. Hashem, T. Schlöder, D. Bléger, W. Wenzel, L. Heinke, *J. Phys. Chem. Lett.* **2019**, *6626*.
- [167] L. Vetráková, V. Ladányi, J. Al Anshori, P. Dvořák, J. Wirz, D. Heger, *Photochem. Photobiol. Sci.* **2017**, *16*, 1749.
- [168] N. A. Voloshin, A. V. Chernyshev, S. O. Bezuglyi, A. V. Metelitsa, E. N. Voloshina, V. I. Minkin, *Russ. Chem. Bull.* **2008**, *57*, 151.